NASA TECHNICAL MEMORANDUM

NASA TM X-62,242

NASA TM X-62,242

UNSTEADY TURBULENT BOUNDARY-LAYER ANALYSIS

R. E. Singleton and J. F. Nash
Lockheed-Georgia Research Laboratory
Marietta, Georgia

L. W. Carr
Ames Research Center
and
U.S. Army Air Mobility R&D Laboratory
Moffett Field, Calif. 94035

U. C. Patel
Institute of Hydraulic Research, The University of Iowa
La Jolla Calif. 92037

(NASA-TM-X-62242) UNSTEADY TURBULENT BOUNDARY LAYER ANALYSIS (NASA) 69 p HC $5.50 CSCL 20D

N73-19297

Unclas
G3/12 65200

February 1973

CONTENTS

LIST OF FIGURES

LIST OF FIGURES (Cont'd)

SYMBOLS

A, A_0, A_1	Constants in external velocity definitions
a_1, a_2	Constants in turbulent energy equation
c	Chord length assumed to be unity
L	Dissipation length
p	Static pressure
P	Period
Q	Velocity magnitude
R	Ratio of local acceleration to substantial acceleration
t	Time
U	Chordwise ensemble average velocity
V	Normal ensemble average velocity
W	Spanwise ensemble average velocity
u	Chordwise random fluctuation about U
v	Normal random fluctuation about V
w	Spanwise random fluctuation about W
$\overline{uv}$	Ensemble average of the product uv
$\overline{vw}$	Ensemble average of the product vw
x	Distance measured in chordwise direction
y	Distance measured normal to wall
z	Distance measured in spanwise direction
Λ	Sweep angle

SYMBOLS (Cont'd)

δ	Boundary-layer thickness
δ^*	Boundary-layer displacement thickness
ρ	Density
τ	Shear Stress
Γ	Empirical constant
Φ_x	$= \Gamma[(\overline{uv}^2 + \overline{vw}^2)^{1/2}(\partial U/\partial y) + \overline{uv}\{(\partial U/\partial y)^2 + (\partial W/\partial y)^2\}^{1/2}]$
Φ_z	$= \Gamma[(\overline{uv}^2 + \overline{vw}^2)^{1/2}(\partial W/\partial y) + \overline{vw}\{(\partial U/\partial y)^2 + (\partial W/\partial y)^2\}^{1/2}]$
ω	Frequency of freestream flow

Subscripts

e	Value at the outer edge of boundary layer
x, z	Component in x- and z- direction
w	Value at wall
o	Value at start of turbulent boundary layer

UNSTEADY TURBULENT BOUNDARY-LAYER ANALYSIS

By

R. E. Singleton*, J. F. Nash*, L. W. Carr**,
and V. C. Patel***

* Lockheed-Georgia Company

** U.S. Army Air Mobility Research and Development Laboratory,
Ames Directorate

*** Institute of Hydraulic Research, The University of Iowa

SUMMARY

The governing equations for an unsteady turbulent boundary layer on a swept infinite cylinder, composed of a continuity equation, a pair of momentum equations and a pair of turbulent energy equations which include upstream history efforts, are solved numerically. An explicit finite difference analog to the partial differential equations is formulated and developed into a computer program. Calculations were made for a variety of unsteady flows in both two and three dimensions but primarily for two dimensional flow fields in order to first understand some of the fundamental physical aspects of unsteady turbulent boundary layers. Oscillating free stream flows without pressure gradient, oscillating retarded free stream flows and monotonically time-varying flows have all three been studied for a wide frequency range. It was found that to the lowest frequency considered, the lower frequency bound being determined by economic considerations (machine time), there weresignificant unsteady effects on the turbulent boundary layer.

The expected phase shifts in wall shear stress and displacement thickness were found, as observed by other investigators. Besides the indirect effect of unsteadiness via the pressure gradient, the turbulent boundary layer is apparently affected directly by the unsteadiness. This effect is clearly seen in flows approaching zero wall shear stress conditions. Unsteady turbulent boundary layers were able to penetrate deeper into the adverse pressure gradient whether or not the pressure gradient was alleviated by unsteady free stream effects (i.e., onset of zero wall shear stress was delayed in either case compared to quasi-steady turbulent boundary layers). For some flow cases, the differences were quite large at high frequencies. The unsteady displacement thickness and wall shear stress approached the zero wall shear stress condition quite differently from the approach of the corresponding quasi-steady values to separation (i.e. no singular behavior was apparent in the unsteady case). For the oscillatory flow cases considered, the quasi-steady wall shear stress values were a good approximation to the corresponding unsteady values for the entire frequency range considered, provided the flow was nowhere close to zero wall shear stress conditions. For these same frequency ranges, the same cannot be said of the displacement thickness values, however. The displacement thickness was not represented well by the quasi-steady model even at relatively low frequencies.

INTRODUCTION

Time-dependence is a conspicious feature of the flow over a helicopter rotor in translating motion, and it has long been suspected that the effects of time-dependence might play an important role in the development of the boundary-layer on such a rotor. This suspicion was heightened when it was found (ref. 1) that quasi-steady calculations of the boundary-layer development indicated gross separation over nearly one-half of the blade disc of a rotor which was known, from experiment, to be unstalled. Although the pessimistic outcome of these calculations could not unquestionably be attributed to unsteadiness in the boundary-layer, it was clear that a study of the effects of time-dependence was urgently needed in order to help isolate the important ingredients of this area of rotor aerodynamics.

The study of the unsteady turbulent boundary-layer is, of course, important in a wider context too. Dynamic stall affects, not only helicopter rotors, but also the blades of turbines and compressors, and the aerodynamic surfaces of aircraft in maneuvering flight. Finally, but not of least significance, the subject is of substantial fundamental interest, and a greater understanding of it can be expected to assist indirectly in the understanding of a much wider range of boundary-layer flows.

The subject of unsteady boundary layers is in its infancy, and the subject of unsteady turbulent boundary layers was virtually untouched until the last three or four years. Since then the differential method of Patel and Nash (ref. 2), and the integral method

of McDonald and Shamroth (ref. 3), for calculating two-dimensional flows with both spacial and temporal variations, have been published. A few other methods have also appeared which treat only temporally-varying flows (refs. 4, 5).

One objective of this work was to develop further the method of Patel and Nash, and extend it to infinite-yawed-cylinder flows as well as two-dimensional flows. A few calculations have been done using this new capability. The second objective was to perform numerical experiments to explore some of the properties of time-dependent turbulent boundary layers, especially those which relate to unsteady separation and dynamic stall. Within the scope of this latter objective it was considered important to try to determine the range of validity of quasi-steady methods. Time-dependent calculations are more difficult to perform and are more expensive to perform than steady ones, and it is helpful to know the point, in terms of increasing unsteadiness of the flow, beyond which the added complexity and expense have to be incurred in order to obtain useful results.

DESCRIPTION OF THE METHOD

Nature of the Flow Considered

The method is designed to calculate the time-dependent, incompressible, turbulent layer on an infinite yawed cyclinder. Cartesian coordinates are placed on the developed surface of the cylinder (whose radius of curvature is assumed to be everywhere large compared with the local boundary-layer thickness); x is measured normal to the generators, y normal to the surface, and z along the generators.

The velocities in the x-, y-, and z- directions are expressed in the form $U + u$, $V + v$, $W + w$, respectively, where U, V, W, u, v, w are all functions of x, y and t. They are not functions of z because the flow is assumed to be invariant in the direction parallel to the generators of the cylinder (ref. 6). The components of velocity $U(x,y,t)$ $V(x, y, t)$, $W(x, y, t)$ are defined as ensemble averages, taken over a large number of realizations of the same basic flow, or successive flows with the same time-history and the same boundary conditions, e.g. successive cycles of a stable oscillatory flow. The components u, v, w represent the random fluctuations about U, V, W, and by implication the ensemble averages of u, v, w are identically zero.

Governing Equations

The equations of motion for a flow of the type described above can be derived from the time-dependent Navier-Stokes equations by replacing the three velocity components by

$U + u$, $V + v$, $W + w$ (as defined above) and forming the ensemble average of the resulting set. Introduction of the boundary-layer approximations, and restriction to flows with zero z- derivatives, then yields the two momentum equations for U and W

$$\frac{\partial U}{\partial t} + U \frac{\partial U}{\partial x} + V \frac{\partial U}{\partial y} + \frac{1}{\rho} \frac{\partial p}{\partial x} + \frac{\partial}{\partial y} \left(\overline{uv} \right) = 0$$

$$\frac{\partial W}{\partial t} + U \frac{\partial W}{\partial x} + V \frac{\partial W}{\partial y} + \frac{\partial}{\partial y} \left(\overline{vw} \right) = 0$$

together with the statement that the pressure is constant through the boundary layer. In the two momentum equations, $\overline{uv}$, $\overline{vw}$ are the ensemble averages of the products uv, vw, respectively, and have essentially the same meaning as the Reynolds stresses appearing in the steady turbulent boundary-layer equations. Thus the shear stresses τ_x τ_z are given by $\tau_x = -\rho \overline{uv}$ and $\tau_z = -\rho \overline{vw}$

The continuity equation retains its usual form

$$\frac{\partial U}{\partial x} + \frac{\partial V}{\partial y} = 0$$

The above equations are identical to the ones that would have been derived if U, V, W had been specified as time averages. However, in order to define time averages, it is necessary to make the stipulation that the time scale of the turbulent motion is short compared with the time scale of the motion as a whole (ref. 3). A number of flows of practical interest involve unsteadiness of the boundary conditions which is too rapid for an adequate distinction to be made, particularly when due attention is paid to the importance of the large-eddy motions in the boundary layer. These motions can have a time scale comparable to the time taken for a particle to be convected a distance many times the boundary-layer thickness.

To state, as we have done here, that the equations involve ensemble-average, rather than time-average, quantities, does not mean that it will not be necessary, in due course, to make the assumption that ensemble averages can be approximated by time-averages. The important point to be made, at this stage, is that the equations are most secure when viewed as ensemble-average equations.

The turbulent shear stresses are assumed to behave according to the rate equations used in the method for steady three-dimensional flows (refs. 6, 7), but with the convective derivative extended to include the time derivative:

$$\frac{\partial}{\partial t}\left(\overline{uv}\right) + U\frac{\partial}{\partial x}\left(\overline{uv}\right) + V\frac{\partial}{\partial y}\left(\overline{uv}\right)$$
$$+ 2a_1\left[\left(\overline{uv}^2 + \overline{vw}^2\right)^{1/2}\frac{\partial U}{\partial y} + \Phi_x + \frac{\partial}{\partial y}\left(a_2\overline{uv}\right)\right.$$
$$\left. + \frac{\overline{uv}}{L}\left(\overline{uv}^2 + \overline{vw}^2\right)^{1/4}\right] = 0,$$

$$\frac{\partial}{\partial t}\left(\overline{vw}\right) + U\frac{\partial}{\partial x}\left(\overline{vw}\right) + V\frac{\partial}{\partial y}\left(\overline{vw}\right)$$
$$+ 2a_1\left[\left(\overline{uv}^2 + \overline{vw}^2\right)^{1/2}\frac{\partial W}{\partial y} + \Phi_z + \frac{\partial}{\partial y}\left(a_2\overline{vw}\right)\right.$$
$$\left. + \frac{\overline{vw}}{L}\left(\overline{uv}^2 + \overline{vw}^2\right)^{1/4}\right] = 0$$

where Φ_x, Φ_z are given by Equation (12) of Reference 7, which leads to co-directionality of the shear stress "vector" and the rate-of-strain vector. The assumption of co-directionality can be relaxed, if desired, by putting

$$\Phi_x = \Phi_z = 0.$$

The functions a_1, a_2, and L are assumed to be the same functions as appear in the steady-flow method (References 6, 7); a_2 and L are shown in Figure 1, and $a_1 = 0.15$. This assumption implies (a) that the ensemble-average quantities $\overline{uv}$, $\overline{vw}$ can be approximated by the time-average Reynolds stresses, and (b) that time-dependence in the mean flow has a negligible effect on the structure of the turbulence*. Neither of these hypotheses has been verified experimentally, and clearly there is an urgent need to do so. For the present, these hypotheses have to be made in order to proceed at all, but it must be stressed that some of the conclusions from this study may need revision if later experimental work shows that certain underlying assumptions in the method are seriously in error.

Method of Solution

The governing equations consist of two momentum equations, for U and W, the continuity equation, and two rate equations for $\overline{uv}$ and $\overline{vw}$. This set of equations is hyperbolic, and is integrated in a three-dimensional domain (x, y, t) by means of an explicit finite-difference method. The calculation scheme is illustrated in Figure 2. The overall scheme is similar to that used by Patel and Nash (Reference 2); values of all the

*The turbulent energy equation does allow for inertia in transfer of information (energy from mean flow to eddy to heat), but the mechanism itself is not a function of the unsteadiness.

dependent variables are calculated over successive planes, t = constant, and the calculation advances in the t-direction. In the present method, however, the dependent variables include W and $\overline{vw}$ in addition to U, V and $\overline{uv}$. In addition, the present method involves a more sophisticated numerical scheme (Reference 8), and a more flexible integration domain; the height of the domain is allowed to vary with x as well as t (Figure 3).

Boundary conditions for the calculation consist of:

- o initial profiles of U, W, $\overline{uv}$, $\overline{vw}$ versus y for t = 0 and all x,
- o initial profiles of U, W, $\overline{uv}$, $\overline{vw}$ versus y for x = 0 and all t,
- o $\frac{\partial U}{\partial y} = \frac{\partial W}{\partial y} = \frac{\partial \overline{uv}}{\partial y} = \frac{\partial \overline{vw}}{\partial y} = 0$, and

  $\overline{uv} = \overline{vw} = 0$

  at $y = 1.25\delta$, 1.25δ being the local height of the integration domain, which varies with both x and t.
- o appropriate boundary conditions at y = 0.

The wall boundary condition is handled in the same way as in the steady-flow method (refs. 6, 7). The outer numerical calculation is matched to an approximate solution, based on the law of the wall, at $y/\delta = 0.05$.

The numerical scheme for the outer layers, $0.05 \leq y/\delta \leq 1.25$, is equivalent to the one-step staggered-mesh scheme described in Reference 8 and is identical to the scheme used in the steady-flow method (refs. 6, 7).

Five-point central differences are used for the y-derivatives, and either 2- or 3-point backward differences for the x-derivatives; backward differences have to be used for $\partial/\partial x$, if the U-component of velocity is positive, to avoid the upstream propagation of information.

The maximum permissible t-step is dictated by stability considerations. In most situations the t-step is roughly proportional to the smallest value of δ at the particular t-station usually δ at $x = 0$. As a result, the computation time varies inversely as the thickness of the upstream boundary layer; the smaller the value of δ at $x = 0$, the longer the run. Figure 4 shows some typical run times on a Univac 1106 computer. For most of the calculations, $\delta_{x=0}$ was taken to be 0.00444, since this value is used in Ref. 2, giving a typical computation of about 5 minutes.

For initial boundary-layer thicknesses much smaller than this, the run times become excessive, and a scheme was developed for segmenting the integration domain so as to reduce them. If δ increases substantially from $x = 0$ to $x = 1$ (as it generally does if $\delta_{x=0}$ is small), the computation is inefficient if a constant t-step, determined from $\delta_{x=0}$, is used for all x. A continuously variable t-step would be awkward to work with, but it is possible to segment the calculation and use a different (constant) step-length in each segment. In the scheme tried, segments were chosen such that the step-length increased by a factor of 3 from each segment to the next. The factor of 3 meant that the integration mesh in any one segment merged smoothly into that in the adjacent one upstream. Figure 4 shows that the scheme was successful in reducing the longest computer times, but it could not reduce the shorter ones because the growth of the boundary-layer thickness was usually insufficient to permit more than one or two segments.

Comparison with Forward Marching Method

To qualify the accuracy of the computer program, sample calculations were carried out for both two-dimensional and swept infinite cylinder flow fields in the time-relaxation mode, in which the boundary conditions are held constant and a steady-state solution is approached asymptotically for "large" times. In practice, "large times" turned out to be about 2.5 time units, where a time unit is the time required for a fluid particle traveling with some defined characteristic velocity to move a distance of one chord length. The results were compared to solutions obtained by the more conventional forward-marching procedure and the correlation is at least as good as that obtained previously by Patel and Nash (Reference 2).

Figures 5 and 6 show the results of a comparison between the two methods for the case of flow over an infinite yawed cylinder, where the chordwise pressure gradient $\left(\partial p/\partial x\right)$ is favorable over the forward part of the cylinder and adverse over the rear. In Figures 5 and 6, all lengths (x, y, δ^*) are made dimensionless by division by the chord-length of the cylinder, velocities by division by Q_{e_o} (the free-stream velocity at infinity), and shear stresses by division by $\rho Q_{e_o}^2$. Figure 5 shows the predicted chordwise variations of δ^*, τ_{w_x} and τ_{w_z}. The greatest discrepancies between the two solutions are 1.2% in τ_{w_x} (at x = 0.26) and 3.0% in δ^* (at x = 1.0). Figure 6 shows the predicted chordwise and spanwise velocity profiles at x = 1, and it is evident, again, that the two methods produce nearly identical solutions.

Based on these results, and similar results for two-dimensional flows, it was concluded that the computer program was performing satisfactorily for flows in which the boundary

conditions are held constant with time. There was no reason to suppose that the same would not be true also for flows with time-varying boundary conditions, and it was decided to proceed to the calculation of fully unsteady turbulent boundary layers.

COMPUTATIONAL EXPERIMENTS

The properties of time-dependent turbulent boundary layers were studied by carrying out computational experiments using the calculation method described in the preceding sections. Five flow situations were selected, designated Flows A through E, and calculations were done for each flow for a range of relevant parameters. Most of the calculations were for two-dimensional flows, although an infinite-yawed-cylinder version of Flow A was examined and the results are included here. Flows A and B were oscillatory flows; Flows C and D were monotonically time-varying, while in Flow E the external flow was first varied monotonically and subsequently held steady allowing a relaxation of the boundary layer towards equilibrium conditions.

The calculations are discussed in detail below, and the results are presented in Figures 7 through 27. In these figures, as before, lengths are made dimensionless by division by the length of the plate on which the flow is developing (unity), velocities by division by Q_{e_o} (which is equal to U_{e_o} in the case of two-dimensional flows), and shear stresses by division by $\rho Q_{e_o}^2$ (or $\rho U_{e_o}^2$ in two dimensions). Time is made dimensionless by multiplication by U_{e_o} and division by the length of the plate. For the oscillatory flows a reduced frequency, ω, is defined as

$$\omega = 2\pi/P$$

where P is the period of the motion in time units. If $\omega = 2\pi$, a complete cycle takes place in the time taken for a fluid particle, moving with velocity U_{e_o}, to be convected the length of the plate. In the monotonically time-varying flows, ω is retained as a measure of the rate of distortion of the flow, i.e. $1/\omega$ is a characteristic time of the motion.

Oscillating Flows Over Flat Plates

The flow A is defined as a free stream flow oscillating harmonically, according to the equation

$$\frac{U_e}{U_{e_o}} = 1 + A \sin \omega t,$$

over a flat plate. The amplitude, A, and frequence, ω, were varied over a reasonable range to determine their effects on the response of the turbulent boundary layer characteristics to this oscillatory flow field. The initial conditions for this calculation were taken to be the asymptotic steady state solution obtained as time approaches infinity (t = 2.5 is sufficient) for A = 0. The boundary conditions for all time at the entrance station for the boundary layer (x = 0) were set by making $\delta_0 \sim (U_e/U_{e_o})^{-.2}$ and scaling the standard initial profiles accordingly. This condition, in fact, is just the requirement that the entrance conditions respond instantaneously to the edge velocity at any instant of time, i.e. quasi-steady conditions. The Reynolds number based on chord length (unity) was taken to be 10^7 and the initial boundary layer thickness was

.00444. The computer program was allowed to run a few time units ($t = 2$ seems to be sufficient) in order to let transients die out and the output was generated at several chord positions for several periods. Quasi-steady solutions were generated by selecting $\omega t = \text{constant}$ and utilizing the forward marching numerical method for steady-state flows.

Figure 7 shows the results for a ten-fold frequency range at an amplitude, A, of 12.5% and Figure 8 shows the same frequency range at an amplitude of 50%. From Figure 7, it is seen that the unsteady wall shear stress anticipates the quasi-steady values; i.e. there is a phase lead between wall shear stress and the external velocity, U_e. Similar effects have been predicted for oscillatory laminar boundary layers (Reference 9), and for perturbed turbulent boundary layers (Reference 3).

In the laminar case the phase lead increases with frequency, up to a maximum value of $\pi/4$. In the present results, however, the phase lead is considerably smaller than this (see Figure 9). The phase leads predicted here are also smaller than the values calculated by McDonald and Shamroth (Reference 3). Their results may have been compromised by inadequacies in the velocity-profile model used in their integral method, and the disagreement may not put the validity of the present results in question.

At low frequencies, a phase lead is apparent in δ^* also; this phase lead decreases with increasing frequency, and at high frequencies the unsteady δ^* actually lags behing the quasi-steady values. The average level of δ^*, for the unsteady flow, increases with both increasing frequency and increasing amplitude, until the average unsteady δ^* is more than twice the average quasi-steady δ^* when $A_1 = 0.5$ and $\omega = 15.7$ (Figure 8).

At the 50% amplitude change (Figure 8) the phase lead in the unsteady wall shear stress appears to decrease more with increasing frequency than at the 12.5% amplitude change. A peculiar skewing appears in the δ^* curve at the higher amplitude although the shear stress curves still remain symmetric about their mean values. Apparently, for this case the various states the turbulent boundary layer passes through at each instant of time due to a change in the external velocity are not reversible when the external velocity change is reversed. This situation occurs whenever the condition of zero wall shear stress is approached as is the case in Figure 8. The δ^* variation for the high frequency case in Figure 8 can be approximately represented by a model in which the velocity profile moves in lock-step with the external flow. Such a model would be valid as $\omega \to \infty$, when $\partial U/\partial t$ would dominate the other terms in the equations of motion. This "high-frequency approximation" allows the statement $U_e \delta^* = \text{constant}$. This result is shown in Figure 8, the constant having been determined for the best curve fit; it works equally well for the lower-amplitude case shown in Figure 7. Whereas the displacement thickness is well represented by the high-frequency approximation, the wall shear stress continues to be well represented by the quasi-steady approximation, and it is remarkable that it works well over such a wide range of both frequency and amplitude.

Figures 9 through 12 show a comparison of the turbulent results with the laminar results of Lighthill (Ref. 9). In Figure 9, a comparison is given of the laminar wall shear stress phase lead with the turbulent values versus the reduced frequency, ω. The turbulent wall shear stress phase lead is much reduced from the laminar values. Figure 10 shows a comparison of the laminar shear stress with the turbulent values versus reduced frequency, ω. Three curves are shown for each case corresponding to three values of the argument ωt. The values for the high frequency approximation in the laminar case when $\omega t = \pi$ or

$3\pi/2$ are identical and consequently are shown as only a dashed curve. The turbulent boundary layer results display the same trends as in the laminar case. The Figures 11 and 12 give graphs of the displacement thickness values analogous to the Figures 9 and 10. Once again it is seen that the turbulent boundary layer results display the same trends as in the laminar case.

A variation of the flow A is that of a swept infinite flat plate immersed in a flow oscillating harmonically in the chordwise direction only, according to the equations

$$\frac{U_e}{Q_{e_o}} = \left[1 + A \sin \omega t\right] \cos \Lambda$$

$$\frac{W_e}{Q_{e_o}} = \sin \Lambda$$

where Q_{e_o} is the velocity magnitude at $t = 0$ and Λ is the sweep angle. Results of this calculation are shown in Figure 13 for the 50% amplitude change. The curves for δ^* and $(\tau_w)_x$ have the same characteristics as in the two-dimensional case with the exception of the skewing of the chordwise wall shear stress at the higher frequency value. This result is probably accentuated by the closeness of the chordwise wall shear stress to zero. However, the spanwise wall shear stress, in contrast to the chordwise wall shear stress, lags the quasi-steady values and this phase lag apparently increases with increasing frequency.

Oscillating Retarded Flows

The flow B is an oscillating retarded flow field defined by the equation

$$\frac{U_e}{U_{e_o}} = 1 + (A_o + A_1 \sin \omega t)x,$$

where $A_o = -0.2$. Calculations were made for flow B in the same fashion as for flow A with the exception that the initial conditions were taken to be the steady state solution obtained as time approaches infinity (about 2.5) with $A_1 = 0$. Figure 14 shows the results for an eight-fold frequency range at the trailing edge when the amplitude change, $A_1/(1 + A_o)$, is 12.5% , and Figure 15 shows the results for a ten-fold frequency range at the trailing edge where the amplitude change is 50%.

From Figure 14, in contrast to the oscillating flow on a flat plate, flow B gives an unsteady wall shear stress and displacement thickness which lag their quasi-steady values. Furthermore, this phase lag decreases with increasing frequency. It appears that the average unsteady δ^* is about the same as the average quasi-steady δ^* for the entire frequency range considered. At an amplitude of 12.5% the boundary layer does not come close to zero τ_w anywhere during the cycle. At the higher amplitude of 50%, however, τ_w becomes very small near the "bottom" of the cycle. Moreover, and this is most interesting, the quasi-steady boundary layer would actually separate during this part of the cycle (Figure 15). Thus the unsteady boundary layer manages to remain attached ($\tau_w > 0$) throughout the cycle, even though the maximum instantaneous retardation would be great enough to cause separation if it were maintained for a long time. It is significant that, in the present case, the effect of time-dependence is to delay the onset of

vanishing τ_w whereas the opposite occurs in the case of the oscillating flat plate (Flow A). In that flow, the wall shear stress, at the bottom of the cycle, would eventually decrease to zero if the amplitude were increased sufficiently; on the other hand, quasi-steady calculctions would never indicate separation unless the amplitude were so large as tc stagnate the external flow.

To return to Figure 15, over the part of the cycle where the quasi-steady calculation indicates separation, the quasi-steady values of δ^* are very large. The unsteady values, in contrast, are well behaved throughout the cycle. Figure 15 shows phase lags similar to the lower amplitude case in Figure 14 Again, if points close to zero wall shear stress conditions are excluded, it is remarkable how good an approximation the quasi-steady wall shear stress values are to the unsteady values in a retarded flow field for a wide range of both frequency and amplitude. The results of the high frequency approximation for δ^* ($U_e\delta^* =$ constant) are also shown in Figure 14, and as in Figure 8 the agreement with the calculated results is excellent.

Monotonically Time - Varying Flows

Computational experiments were performed for three flows in which the external velocity varied monotonically with time, instead of sinusoidally as in Flows A and B. The three flows, were two-dimensional, and were defined as follows:

Flow C: $$\frac{U_e}{U_{e_o}} = 1 - \omega t x$$

Flow D: $$\frac{U_e}{U_{e_o}} = 1 + \omega t(1-x)$$

Flow E: $$\frac{U_e}{U_{e_o}} = 1 + \omega t(1-x) \text{ for } 0 \leq t \leq t_f$$

$$\frac{U_e}{U_{e_o}} = 1 + \omega t_f(1-x) \text{ for } t > t_f$$

Only positive values of ω and t were considered, and so all three flows involved decelerating external flows. In Flow C the external velocity distribution "pivoted" about the leading edge of the plate ($x = 0$), and this flow might be regarded as an idealized model of the flow in a channel with one wall pivoted and rotating outwards.

In Flows D and E the external velocity distribution pivoted about the trailing edge of the plate ($x = 1$), and these flows might be regarded as idealized models of the flow over an airfoil pitching continuously (Flow D), or pitching up to some positive angle of incidence and then being held still (Flow E).

The main objective was to determine the onset of zero wall shear stress and to examine the variation of its point of onset with the rate of distortion of the external flow, ω. Small values of ω indicate slow distortion of the external flow, and large values indicate rapid distortion. As $\omega \longrightarrow 0$, steady-flow conditions are approached, and finite values of ωt (i.e. finite values of $\partial U_e/\partial x$) are reached only for "long" times: $t \longrightarrow \infty$. Steady-flow calculations, done for comparison with the time-dependent ones, could be performed either by the time-relaxation process or by a forward-marching procedure. In most cases the latter method was used for reasons of machine economy; the run-time

necessary to reach a steady-state solution in a time-relaxation calculation becomes long because of the long convection times associated with the small velocities in the flow close to separation.

The second objective was to examine the general character of the solut · the hope of shedding some light on the behavior of the unsteady turbulent boundary approaching a point of zero wall shear stress.

The calculations for all three flows were done for a Reynolds number of 10^7 based on U_{e_o} and the length of the plate (unity). The initial conditions at $t = 0$ corresponded to steady, flat-plate flow with $U_e = U_{e_o}$ and on upstream boundary-layer thickness, at $x = 0$ of 0.00444. For Flow C, the external velocity at $x = 0$ was constant for all time, and the assumption of constant boundary-layer thickness at that point seemed reasonable and this was made. However, in Flow D, U_e at $x = 0$ is not constant but increases with time, and the problem of constructing reasonable initial conditions there presented a matter of some concern. It was decided to try to determine the sensitivity of the solution to changes of the initial conditions at $x = 0$. Calculations were done for a few representative cases with initial conditions as follows:

(a) flat-plate velocity and shear-stress profiles with constant boundary layer thickness (= 0.00444),

(b) flat-plate velocity and shear-stress profiles with boundary layer thickness decreased as $(U_e/U_{e_o})^{-0.2}$ to account for the change in local Reynolds number,

(c) velocity profiles, with boundary layer thickness of .0444, generated by adding a constant increment of velocity ($= U_e - U_{e_o}$) at all values of y, to approximate conditions appropriate to $\omega \to 00$; the shear stress profiles for this case were identical to those in (a) except in the immediate vicinity of $y = 0$ (where $\tau_w \to 00$).

In all the cases run, vanishing wall shear stress was predicted to occur, at $x = 1$, at values of ωt which were within 1% of each other for the three sets of starting conditions. The calculations indicated larger boundary-layer thickness (up to 36% larger) when (c) was used, compared to (a) and (b). However, these larger values of δ occurred at small values of x, and the differences were much smaller near $x = 1$. Nearly identical results were obtained with (a) and (b); the predicted values of δ were the same to within 1% for all values of x greater than 0.02.

Thus it appeared that the solution was fairly insensitive to the upstream starting conditions, and that generality of the conclusions from the present work was unlikely to be compromised by an unfortunate choice. It was decided that the assumption of constant δ was reasonable, and this was made in all the subsequent calculations.

Figure 16 shows some results for Flows C and D. The calculations were run until the wall shear stress, τ_w, just reached zero at $x = 1$, and the value of ωt at this instant was recorded; ωt is equal to the instantaneous velocity gradient $-\frac{\partial U_e}{\partial x}$. The ratio of $(\omega t)_{\tau_w = 0}$ to its value when $\omega \to 0$ is plotted as a function of ω in the left-hand diagram. The results show that, for both Flow C and Flow D, τ_w vanishes, at $x = 1$, at a higher

value of ωt than in quasi-steady flow; in other words, there is a delay in the onset of vanishing τ_w. In Flow C, $(\omega t)_{\tau_w = 0}$ increases to a value some 50% greater than that for quasi-steady separation, and then remains approximately constant for $\omega > 0.6$. In Flow D, the value of $(\omega t)_{\tau_w = 0}$ increases continuously with increasing ω, and there is a substantial delay in vanishing τ_w for large values of ω. For example, with $\omega = 10$, $(\omega t)_{\tau_w = 0}$ is some five times greater than it is when $\omega \to 0$ (quasi-steady). At these high values of ωt, the streamwise gradients are so large that the validity of the boundary-layer approximations becomes questionable. For this reason, the results for Flow D, with $\omega > 8$, should be treated with caution, and they are shown by dashed curves in Figure 16. The trend suggests that, for high enough values of ω vanishing wall shear stress might never occur.

One of the effects of time-dependence is to modify the streamwise pressure gradient, $\partial p/\partial x$. For flow over an infinite yawed cylinder, Euler's equation for flow in the external stream takes the form

$$\frac{\partial U_e}{\partial t} + U_e \frac{\partial U_e}{\partial x} + \frac{1}{\rho} \frac{\partial P}{\partial x} = 0$$

The equation shows that $\partial p / \partial x$ can be either increased or decreased, depending on the sign of $\partial U / \partial t$. The quantity R, where

$$R = -\left(\partial U_e / \partial t \right) \Big/ \left(\frac{1}{\rho} \frac{\partial p}{\partial x} \right)$$

is a measure of the contribution of [illegible] to the total pressure gradient.

Positive values of R correspond to cases where $\partial p / \partial x$ is increased, i.e. becomes more adverse, negative values to cases where the adverse pressure gradient is alleviated.

The right-hand diagram in Figure 16 shows the results for Flows C, D ploted versus R. Actually, R is a function of x, and the values plotted correspond to $x = 0.5$. Flow D generates negative values of R and the delay in the onset of zero τ_w takes place in an environment where the adverse pressure gradients are alleviated by the effects of time-dependence. On the other hand, Flow C generates positive values of R and, while the effects are less marked than in Flow D, there is again a delay in vanishing τ_w, and it occurs in the face of an increasingly adverse pressure gradient. Indeed, at the highest value of ω considered the value of $\partial p / \partial x$ is some 300 times greater than was necessary to cause separation of $x = 1$ in steady flow.

The inference is that the augmentation or alleviation of $\partial p / \partial x$ does play a part in the effect of time-dependence on vanishing wall shear stress, but that, at least for flows similar to the present ones, it is not the only factor to be considered. The fact that a delay in vanishing τ_w occurred even when $\partial p / \partial x$ was increased suggests that time-dependence influences the flow directly as well as via $\partial p / \partial x$. It might also be worth mentioning that, regardless of the sign of $\partial U_e / \partial t$ and its effect on $\partial p / \partial x$, the point of vanishing τ_w can move upstream only if $\partial U / \partial t$ in the vicinity of the wall is locally negative.

In Figures 17, 18, τ_w and δ^*, from the calculations for Flow C, are plotted versus x for a low (0.25) and a high (31.4) value of ω. The results correspond to the instant of time, and the instantaneous value of ωt, where τ_w just vanishes at $x = 1$. The results of two quasi-steady calculations are also plotted for comparison. In one, the value of ωt is the same; in the other, the value of ωt is reduced such that separation

occurs at $x = 1$. With ωt the same, separation of the steady boundary layer occurs ahead of $x = 1$ (vanishing wall shear stress is delayed in the unsteady case). In order to obtain separation at $x = 1$, it is necessary to reduce ωt, i.e. to reduce the streamwise adverse pressure gradient.

Figures 19, 20 show the corresponding results for Flow D, again for a low and a high value of ω. It will be noted, in Figure 20 especially, that the values of τ_w for the two quasi-steady runs are substantially different from one another particularly at low values of x. This difference is a consequence of the different levels of U_e between the two quasi-steady flows; in Figure 20, for example, the two values of ωt used in the quasi-steady calculations are different by a factor of 9. Plotting $\tau_w/(\rho U^2_e)$, rather than $\tau_w/(\rho U^2_{e_o})$ would have reconciled the results for small x, but would have obscured important trends near separation.

All four sets of results (Figure 17 through 20) exhibit essentially the same characteristics. The steady-flow separation is associated with increasing values of $-(\partial \tau_w / \partial x)$, as the separation point is approach, reminiscent of the square-root singularity observed in the laminar case. Correspondingly, δ^* increases rapidly, again, in a quasi-singular manner. In contrast, in the time-dependent cases, the approach to zero wall shear stress is more gradual: the value of $-(\partial \tau_w / \partial x)$ <u>decreases</u> rather than increases with x. The results suggest that the delay of vanishing τ_w is directly linked to the absence of the square-root singularity (or something close to it) in the $\tau_w(x)$ variation. The curves of δ^* also depict important differences. Particularly at the higher values of ω, δ^* is smaller and has a markedly smaller slope as τ_w goes to zero. In short, there is no evidence of singular behavior, and thus the results support the views of Sears (Reference 10). It was not possible to continue the calculations beyond the point of instantaneously zero wall shear stress, and so the question of the existence

of a singularity downstream of this point could not be addressed. Neither could calculations easily be done for the situation where the point of zero τ_w is moving <u>downstream.</u> For this case, the Sears model (Reference 10) of unsteady separation would predict that the singularity lies ahead of the point of vanishing τ_w.

The results presented so far, for Flows C, D, all correspond to the instant of time at which $\tau_w = 0$ at $x = 1$. Further studies were conducted to examine the upstream movement of the point of vanishing τ_w to smaller values of x.

Figure 21 shows curves of τ_w versus x for increasing time; these are for Flow D with $\omega = 1.57$. As stated before, τ_w increases rapidly with time, for low values of x, because of the increase of U_e. When τ_w fell to zero at $x = 1$, the row of node points of the integration mesh, corresponding to $x = 1$, was dropped, and the calculation was continued to largervalues of t.

Additional rows of node points were dropped as the point of zero τ_w moved upstream. Figure 22 shows the corresponding curves of δ^* versus x. It will be noted that, up to a time $t = 1.9$, δ^* is independent of time for x less than about 0.2. This result provides indirect confirmation that the assumption of constant δ (and therefore nearly constant δ^*) at $x = 0$ was a reasonable one. It will be noted, also, that the curves become progressively steeper as the point of zero τ_w moves forward. It is not clear, at this stage, whether a singularity is being re-established, or whether this effect is due to numerical error as the result of there being fewer node points left in the integration net.

Figure 23 illustrates the velocity and shear stress profiles calculated for Flow D (with $\omega = 1.57$) at $x = 0.67$. The wall shear stress vanishes at $x = 0.67$ when $t = 1.93$,

i.e. when ωt is approximately 3. Quasi-steady separation would occur at $x = 0.67$ only if ωt were reduced to 1.55. The profiles corresponding to this latter situation are shown for comparison. It is interesting to note that the velocity profiles are similar in thickness and shape, the only significant difference being the edge velocity, U_e; thus plots of U/U_e versus y would look almost identical. Furthermore, the shear stress profiles are similar in shape and would fall close to one another if plotted in terms of $\tau/(\rho U_e^2)$.

This similarity in shape is surprising in view of the difference in behavior of $\tau_w(x)$ and $\delta^*(x)$ as the point where $\tau_w = 0$ is approached.

The same time-dependent flow (Flow D, with $\omega = 1.57$) reaches $\omega t = 1.55$ when t is approximately one. The profiles corresponding to this condition are shown in Figure 23 for comparison both with the quasi-steady results, at the same ωt, and with the results for Flow D at the later time, $t = 1.93$. The comparison shows that the two velocity profiles with the same edge velocity, U_e, are substantially different in thickness and shape. Moreover, the maximum shear stress is quite different.

Thus it would appear that the similarity between time-dependent and quasi-steady flows is closest when they are compared at the points where $\tau_w = 0$ in both, even though the edge velocities are then different and even though the upstream histories of the two flows are radically different. Conversely, development in the same external velocity distribution appears to be largely irrelevant; it does not ensure the same upstream history and does not ensure even approximate similarity between the two flows.

Figure 24 shows the variation with time of τ_w and δ^* at x = 1, for Flow D with $\omega = 1.57$; τ_w goes to zero when t = 1.37. Flow E, the results of which are shown for comparison, is identical to Flow D for $0 \leq t \leq 1$, but for $t > 1$ the external flow is frozen with $\omega t = 1.57$. In Flow E, τ_w goes to zero at t = 1.47.

Figure 25 shows the forward movement of the point of zero τ_w for Flows D, E with $\omega = 1.57$, and also with a higher value, $\omega = 31.4$. In Flow D the external velocity gradient increases continuously, and the point of zero τ_w moves forward continuously at least as far as x = 0.5. The higher the value of ω, the more rapidly this point moves forward. In the case of Flow E, the point of vanishing τ_w moves forward to the position of the quasi-steady separation point for the particular value of ωt; here, around x = 0.67. Thus for $t > 1$ when $\omega = 1.57$, and for $t > 0.05$ when $\omega = 31.4$, the external velocity distribution, $U_e(x)$, is frozen and the movement of the point of zero τ_w is just part of the relaxation towards steady-state conditions. It is interesting to note that the time scale describing this relaxation process appears not to be very dependent on the value of ω corresponding to the previous unsteady external flow. It is also interesting to note the comparatively long time necessary for the flow to settle down to the new steady-state situation, nearly 4 time units, which (at this value of ωt) is roughly five times the time taken for a fluid particle in the external flow to be convected from x = 0 to x = 1.

During the relaxation phase of Flow E, while the external velocity distribution is frozen, the characteristics of this flow have to change from those appropriate to time-varying conditions to those appropriate to steady-state conditions. This process is illustrated by Figure 26 which shows the variation of τ_w and δ^* with x and t for Flow E with $\omega = 1.57$. The shape of the $\tau_w(x)$ curves changes from one in which $-(\partial \tau_w / \partial x)$ decreases with increasing x to one where it increases with x. At the same time, the curves of δ^* versus x become steeper as the point of zero τ_w is approached.

Figure 27 shows the corresponding velocity and shear stress profiles. It is interesting to note how the velocity profile approaches that for steady-state separation by a combination of retardation and thickening which leaves the average velocity gradient, $\partial\bar{u}/\partial y$, nearly constant. The maximum shear stress increases far more than the wall shear stress decreases. It increases roughly in proportion to δ, rather than to δ^2 which would be predicted from mixing-length theory for a boundary layer with a constant $\partial U/\partial y$. This departure from a mixing-length type correlation between the shear stress and the velocity gradient is to be expected in this flow because of the large streamwise gradients.

CONCLUSIONS AND RECOMMENDATIONS

The method developed here for calculating time-dependent turbulent boundary layers in incompressible flow past infinite yawed cylinders is a logical development from the work of Nash and Patel on steady three-dimensional turbulent boundary layers. One of the space dimensions of the integration domain is replaced by time, while the three-dimensionality of the velocity and shear-stress vectors is retained; U, V, W, τ_x, τ_z are determined in the domain (x, y, t).

The empirical content of the method, the dissipation length, diffusion function and the ratio of the shear stress to the turbulent kinetic energy, are carried over from the steady-flow methods. The assumption is made that the original forms of these functions still hold, and the additional assumption is made that the ensemble averages in the time-dependent equations can be approximated by time-averages. These assumptions have not been verified experimentally, and until they are, the conclusions of the present study cannot be accepted without reservation. However, the aim has been to establish trends rather than definitive values, and it is not unreasonable to expect that these trends will survive possible changes in the empirical input which are called for as the result of further experimentation.

It is quite evident, from the results shown, that there are significant unsteady effects on the turbulent boundary layer particularly in the regime of approaching zero wall shear stress. For the oscillatory cases examined, even for the lowest frequencies calculated, there were significant effects on the displacement thickness. A small degree of phase

shift was observed between the wall shear stress and the external velocity. However, the level of wall shear stress differed little from quasi-steady values, corresponding to very low frequency, until zero wall shear stress was approached.

The effect, on the boundary layer, of time-dependence in the external flow is complex, and cannot be represented merely by a change of the streamwise pressure gradient. For some flows the onset of vanishing wall shear stress is delayed, compared with the equivalent steady flow, not only when the adverse pressure gradient is alleviated by the unsteadiness, but even when it is increased. The delay was clearly demonstrated by the monotonically time-varying flow examples where the approach to zero wall shear stress conditions was examined. Unsteady turbulent boundary layers were able to penetrate deeper into adverse pressure gradients (i.e. delayed onset of zero wall shear stress) than could be accounted for by quasi-steady calculations. For some flow cases, the differences were quite large at high frequencies. In addition, the unsteady displacement thickness and wall shear stress approached the zero wall shear stress condition quite differently from the approach of the corresponding quasi-steady values to separation. The results support the contention of Sears (Reference 10) and others that the point of vanishing wall shear stress, in an unsteady boundary layer, is not a singular point. Furthermore, the results suggest that the fact that it is not a singular point has a lot to do with the delay in vanishing wall shear stress mentioned earlier.

This study did not address the question of separation, and we have been careful to avoid any suggestion that the point of vanishing wall shear stress is a separation point in unsteady flow. Indeed, if separation, in the sense of flow detachment, is associated

with singular behavior of the displacement thickness, the present results indicate that separation was always downstream of the point of vanishing wall shear stress for the flows examined. Thus it would appear that separation was delayed even more by the effects of time-dependence than was the onset of vanishing wall shear stress. There is an urgent need for a study of the events surrounding actual separation, i.e. detachment, of the unsteady turbulent boundary layer. With certain modifications the present calculation method could be used to examine the development of the flow between the onset of zero wall shear stress and the onset of separation.

This study has drawn attention to the strengths and also to the weaknesses of the present calculation scheme. The uncertainties associated with the flow model have already been mentioned, but a few comments are in order concerning the numerical scheme for integrating the governing equations. The explicit scheme used here is well tried, having been employed in a range of three-dimensional steady boundary-layer calculations as well as in the present unsteady-flow method. There are deficiencies in the scheme from the standpoint of precision, particularly in the inner-layer calculation; however, the numerical precision is probably at least as good as the accuracy of the empirical flow model. The major disadvantage of the present scheme lies in the long computarion times required. It has not been possible to explore important low frequency ranges because the calculations became too expensive, nor was it possible to treat flows where the boundary-layer thickness at the upstream end of the domain was small. There is an urgent need to improve the economy of the present method, and it would seem that this can be done only by replacing the explicit numerical scheme by an implicit one which makes no demands on step size for stability. The conceptual framework of a suitable

implicit scheme has already been established. Be that as it may, the existing method represents a very useful tool, as it stands, and a number of further investigations can be made even before the implicit method is in an operational state. The tools developed in this analysis should be used to investigate the differences between the turbulent boundary layer produced by an unsteady free stream but stationary wall and a steady free stream but non-stationary wall. Of considerable interest would be the utilization of these tools to calculate unsteady turbulent boundary layers which correspond to the experimental investigations being conducted by the U.S. Army Air Mobility R&D Laboratory and the Naval Postgraduate School in Monterey. The comparison of these experimental data with the theoretical values would not only serve to elucidate unsteady turbulent boundary layers but would also point out ways in which the mathematical model might be improved.

Aside from these fundamental investigations, the tools developed in this research program are ready to and can be utilized to great advantage in studying the practical problem of pitching airfoils and dynamic stall. In particular, an investigation can be carried out on the question of lift coefficient overshoot with regard to when and how does separation occur. Related problems which can be studied are the effect of frequency on displacement effect and the resultant effects on pressure distribution. It is entirely possible that current tools for calculating the unsteady turbulent boundary layer can shed some light on the bursting of the separation bubble. The capability now available for unsteady turbulent boundary layers coupled with advanced methods for treating the potential flow could well answer the question of how the boundary layer rolls up after separating from the pitching airfoil.

The analysis and computer program can and should be extended to compressible flow. When that is accomplished, the required technology for examining the very complex problem of shock-unsteady turbulent boundary layer interaction would be in hand.

SUMMARY OF CONCLUSIONS

1. There are significant unsteady effects on the turbulent boundary layer particularly in the regime of approaching zero wall shear stress.

2. For the retarded free-stream flow case, the effect of time-dependence is to delay the onset of vanishing τ_w whereas the opposite occurs in the case of the oscillating flat plate.

3. Unsteady turbulent boundary layers were able to penetrate deeper into adverse pressure gradients whether or not the pressure gradient was alleviated by unsteady free stream effects (i.e., onset of zero wall shear stress was delayed in either case compared to quasi-steady turbulent boundary layers).

4. The unsteady displacement thickness and wall shear stress approached the zero wall shear stress condition quite differently from the approach of the corresponding quasi-steady values to separation.

5. In contrast to the steady-flow separation, associated with increasing values of $-(\partial\tau_w/\partial x)$, the time-dependent approach to zero wall shear stress is characterized by $-(\partial\tau_w/\partial x)$ decreasing.

6. If separation, in the sense of flow detachment, is associated with singular behavior of the displacement thickness, the present results indicate that separation was always downstream of the point of vanishing wall shear stress for the flows examined.

7. Regardless of the sign of $\partial U_e/\partial t$ and its effect on $\partial p/\partial x$, the point of vanishing τ_w can move upstream only if $\partial U/\partial t$ in the vicinity of the wall is locally negative.

8. For Flow D, the solution was fairly insensitive to the upstream starting conditions allowing the assumption of a constant initial boundary layer thickness to be made.

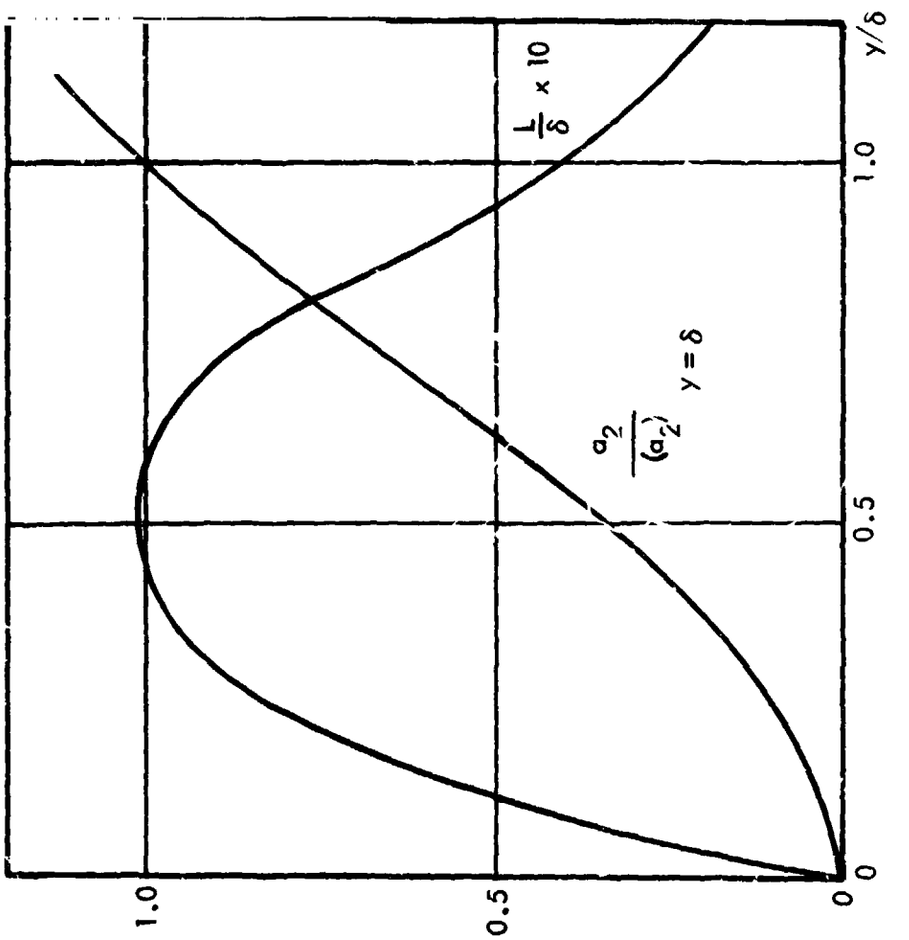

Figure 1. Empirical Functions

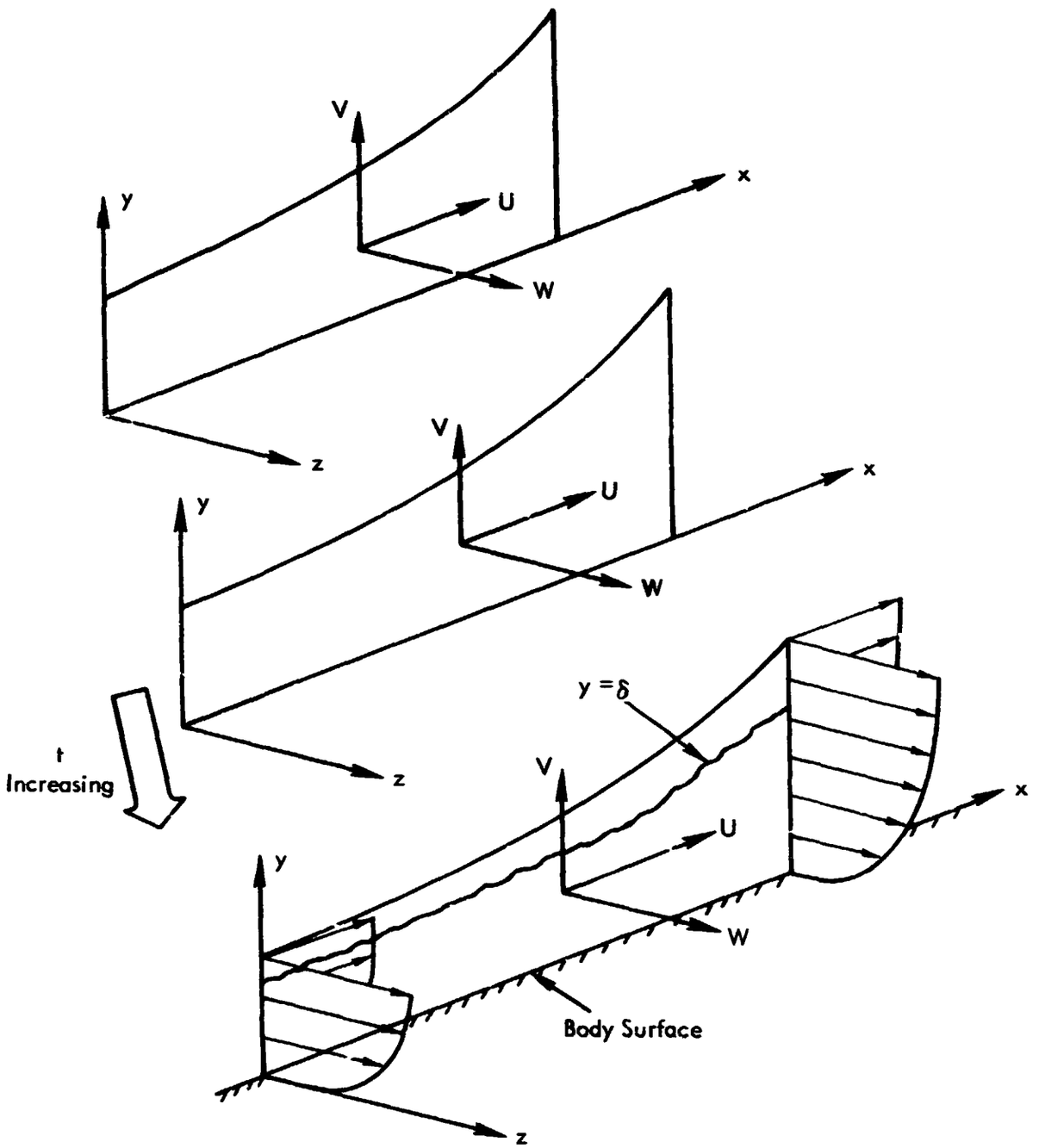

Figure 2. Schematic Representation of the Method of Calculation

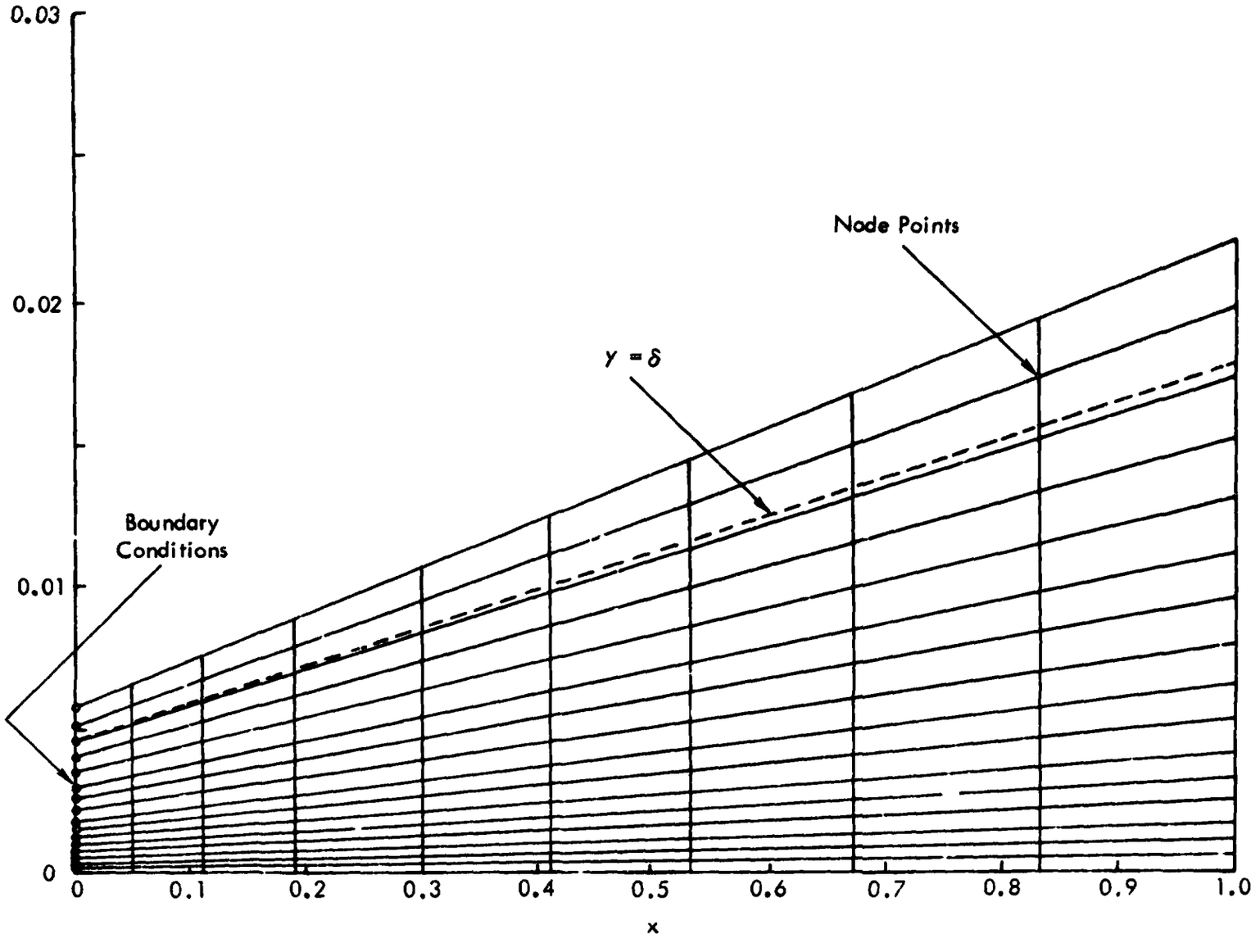

Figure 3. Section x - y of the Integration Domain for a Typical Calculation

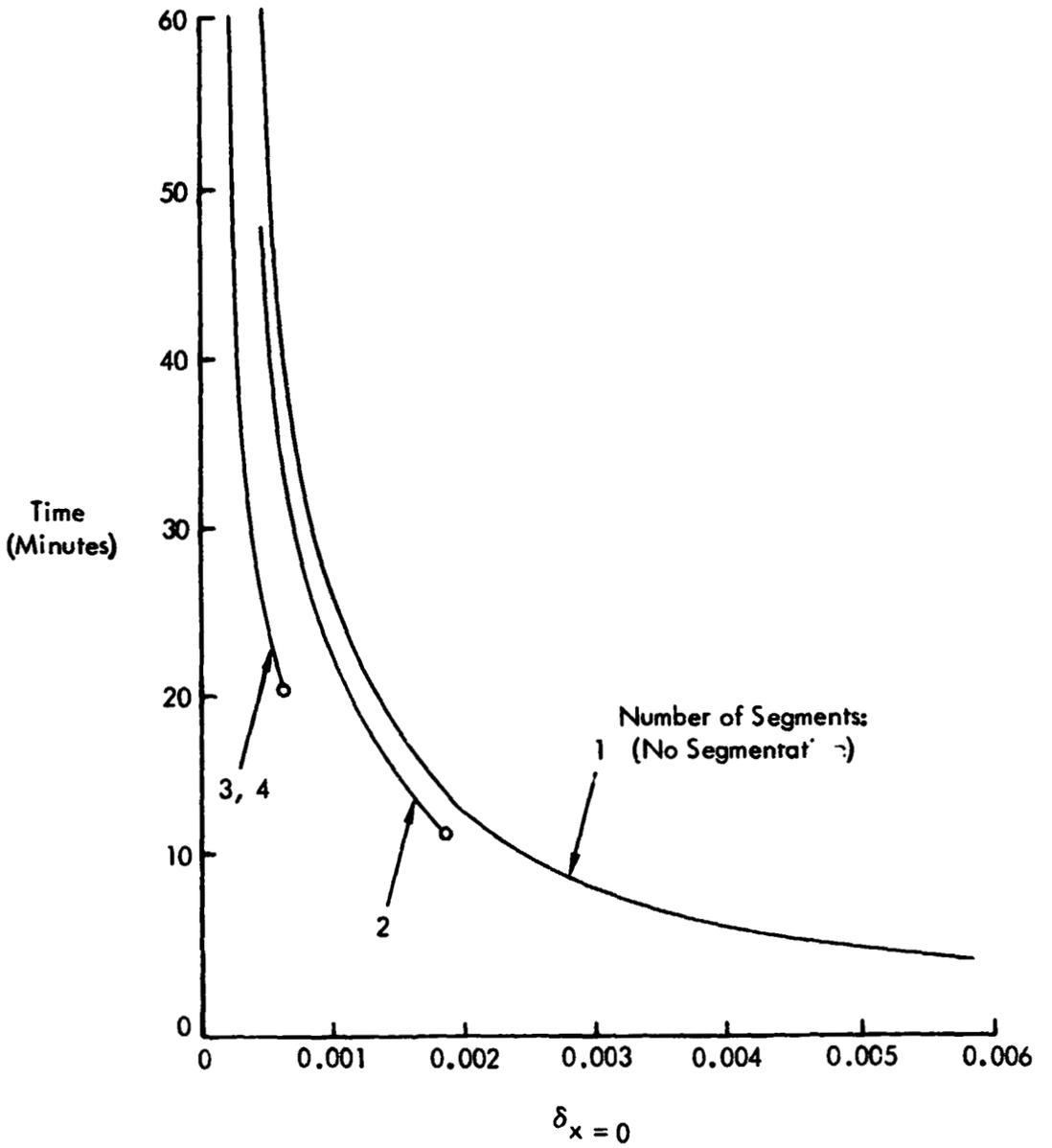

Figure 4. Computation Time for a Typical Calculation

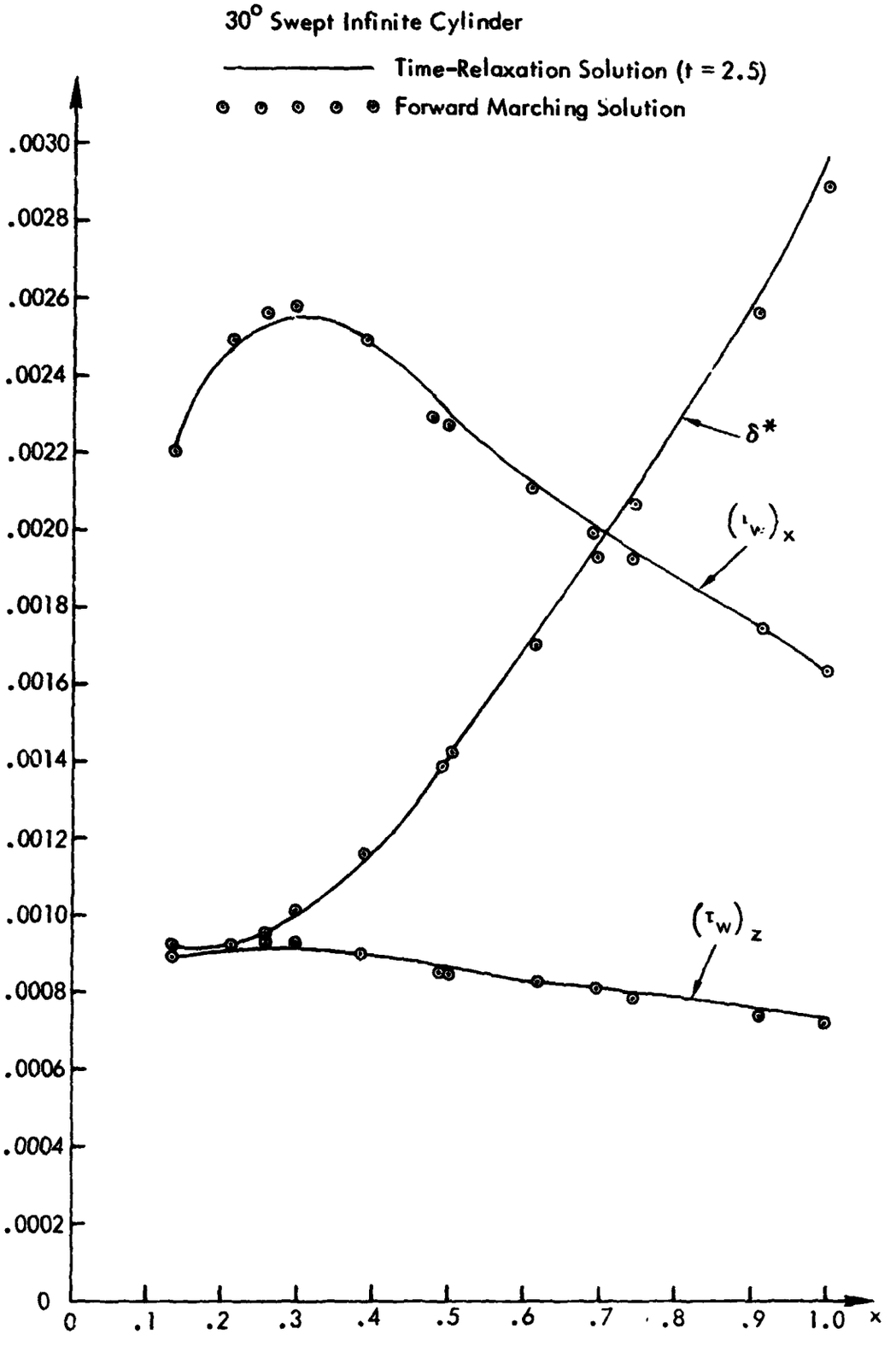

Figure 5. Comparison of Time-Relaxation Results with Forward Marching Results for a 30° Swept Infinite Cylinder

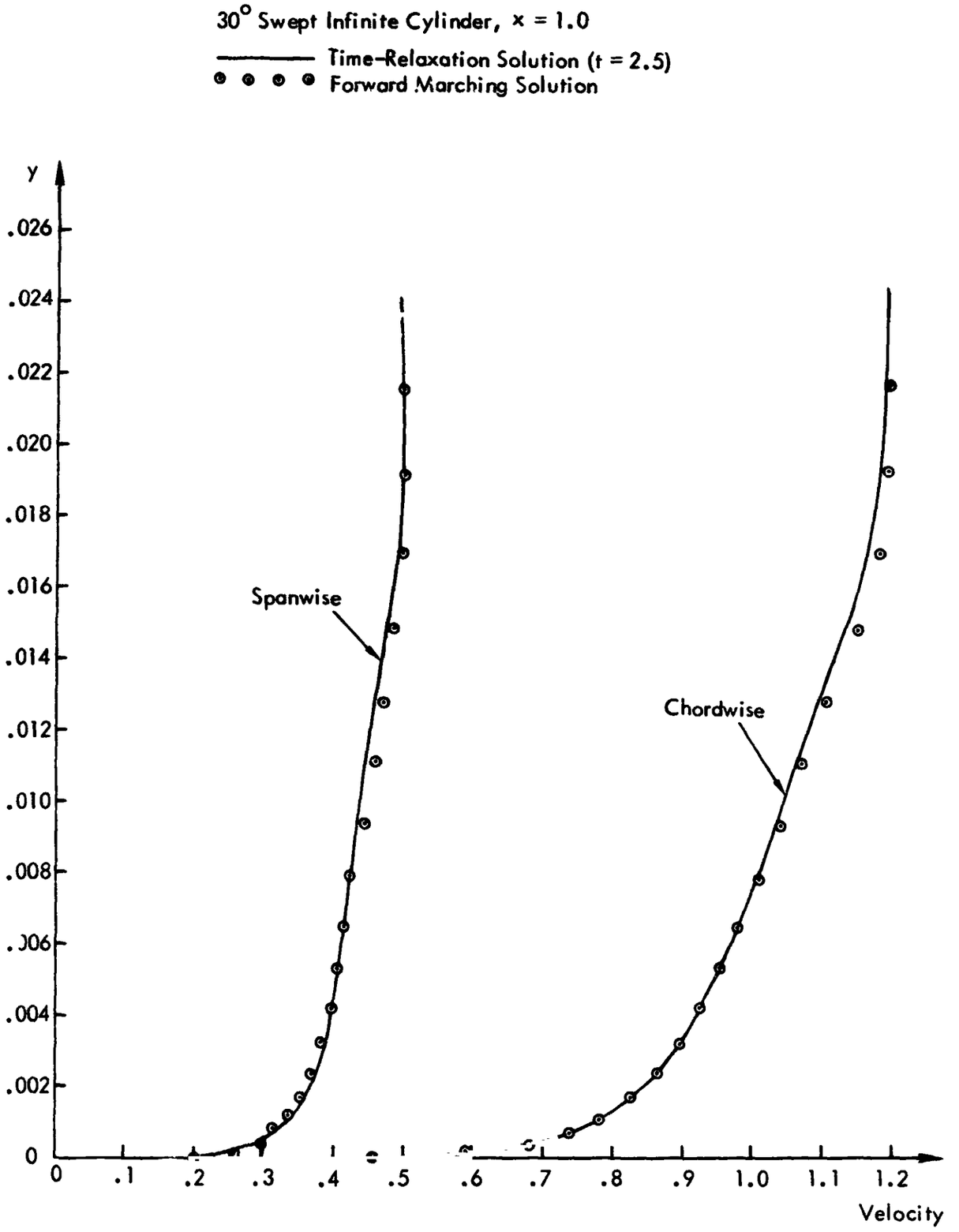

Fig 6. Comparison of Time Relaxation Velocity Profiles with Velocity Profiles Obtained Via Forward Marching Method at the Trailing Edge of a 30° Swept Infinite Cylinder

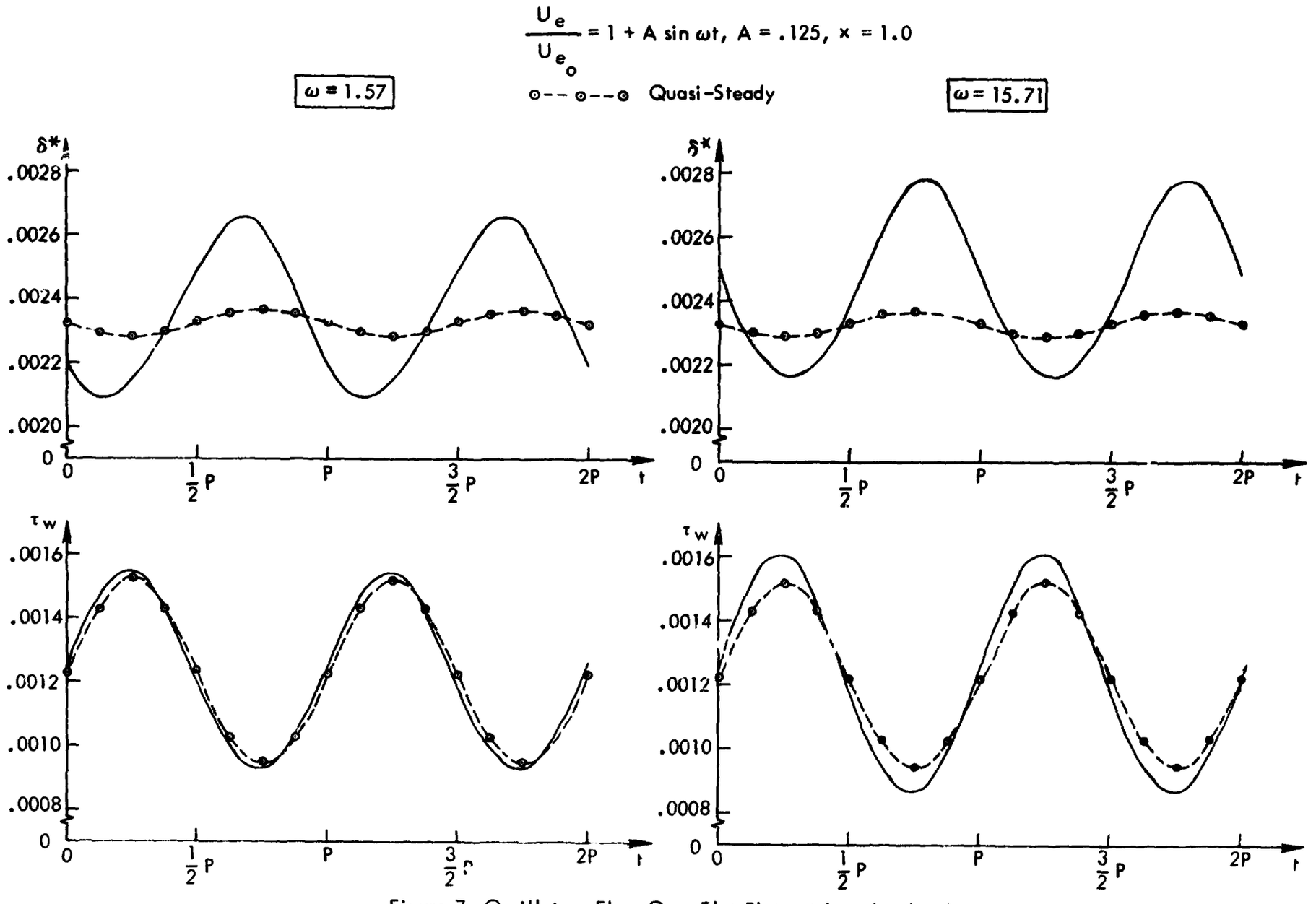

Figure 7. Oscillatory Flow Over Flat Plate at Low Amplitude

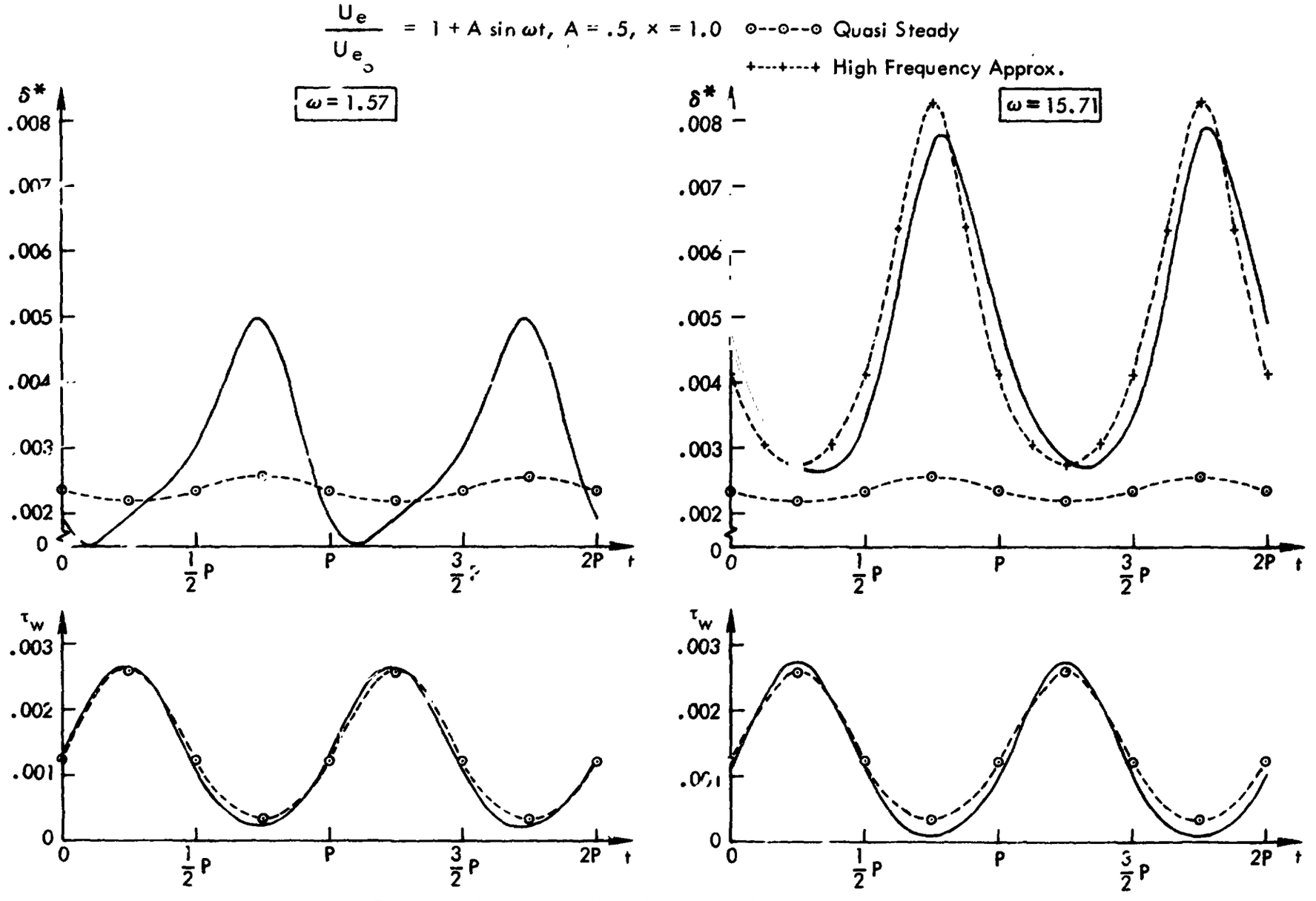

Figure 8. Oscillatory Flow Over Flat Plate at High Amplitude

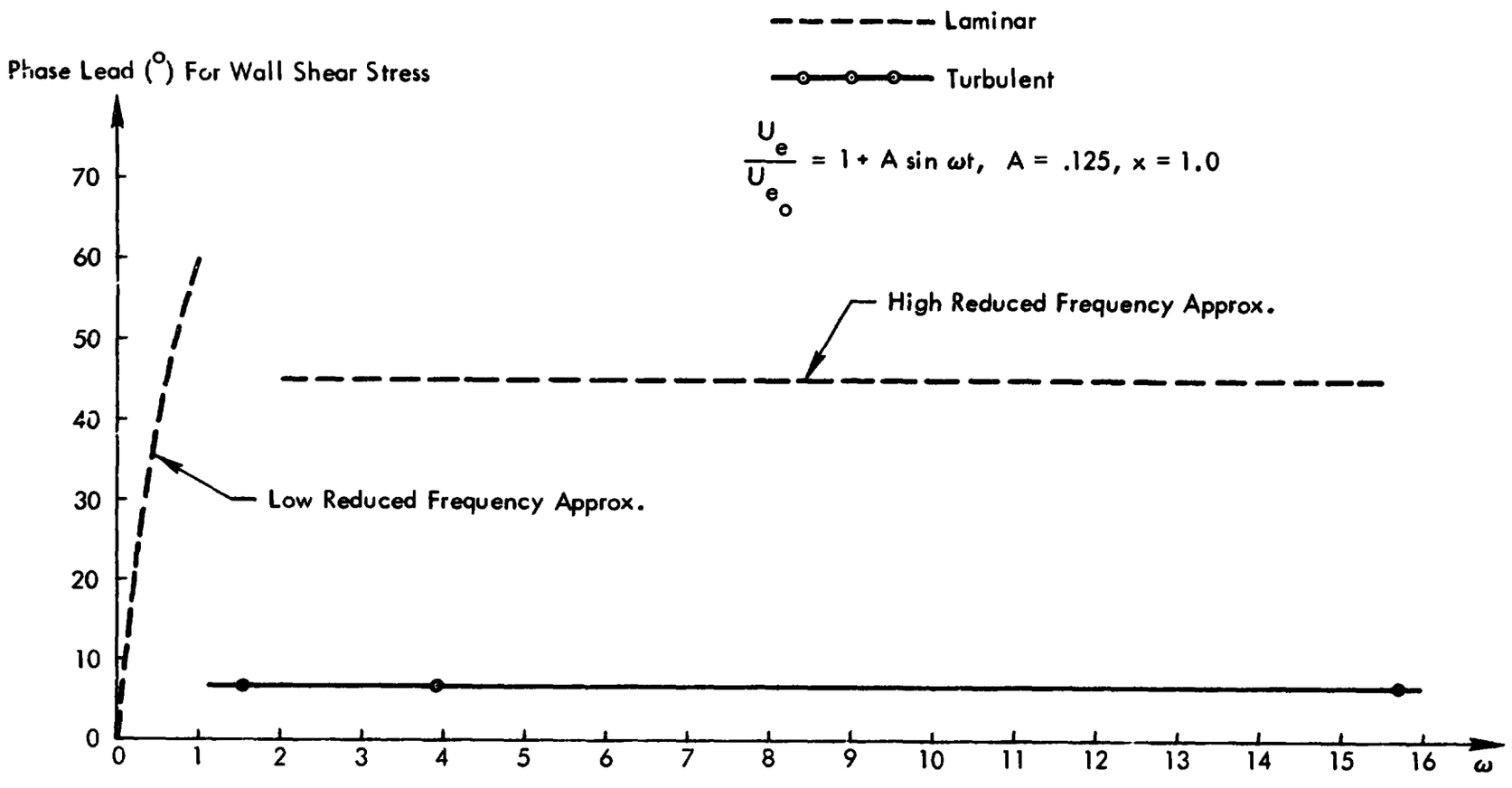

Figure 9. Wall Shear Stress Phase Lead Vs. Reduced Frequency for Laminar and Turbulent Flow

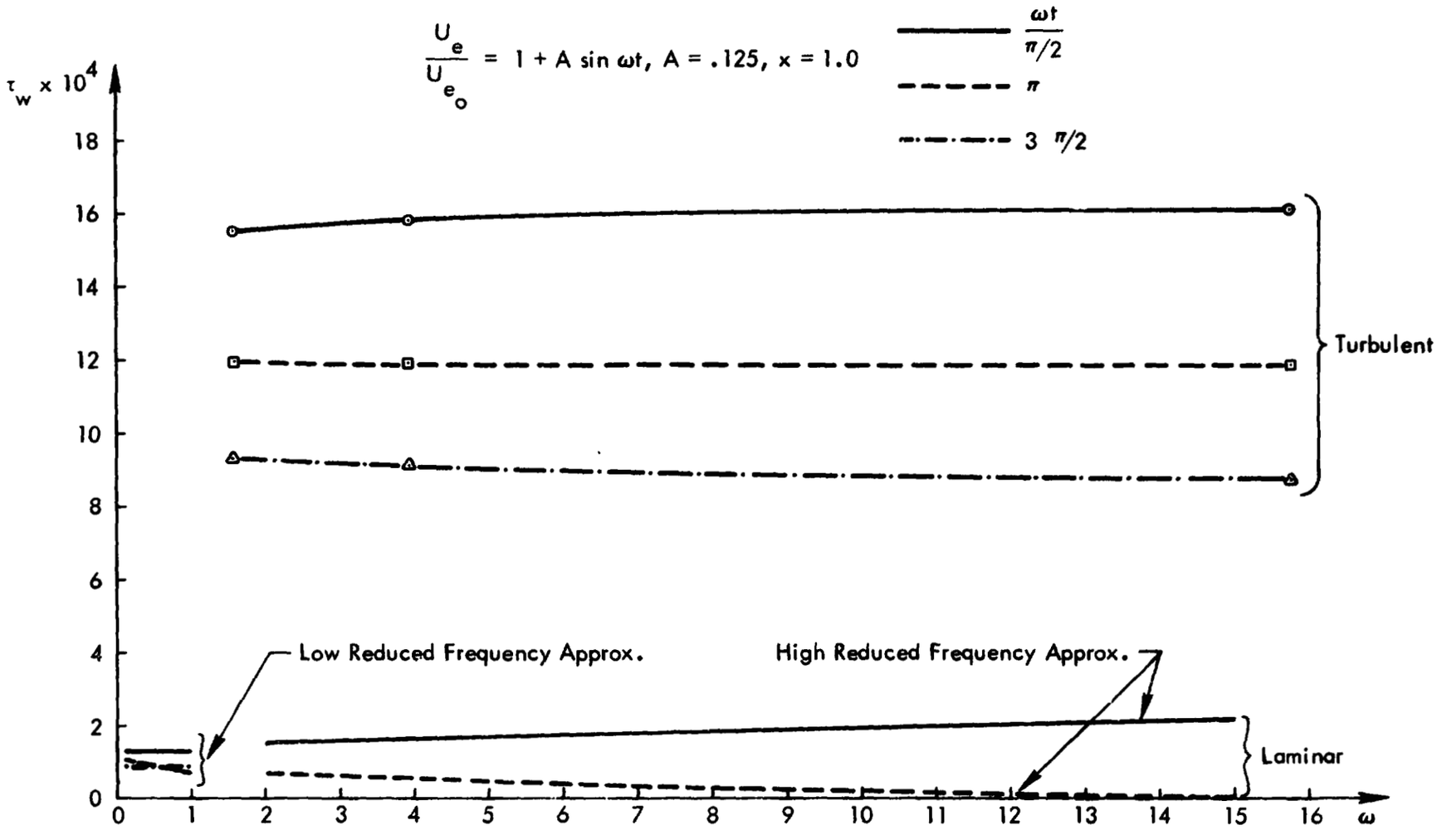

Figure 10. Wall Shear Stress Vs. Reduced Frequency for Laminar and Turbulent Flow

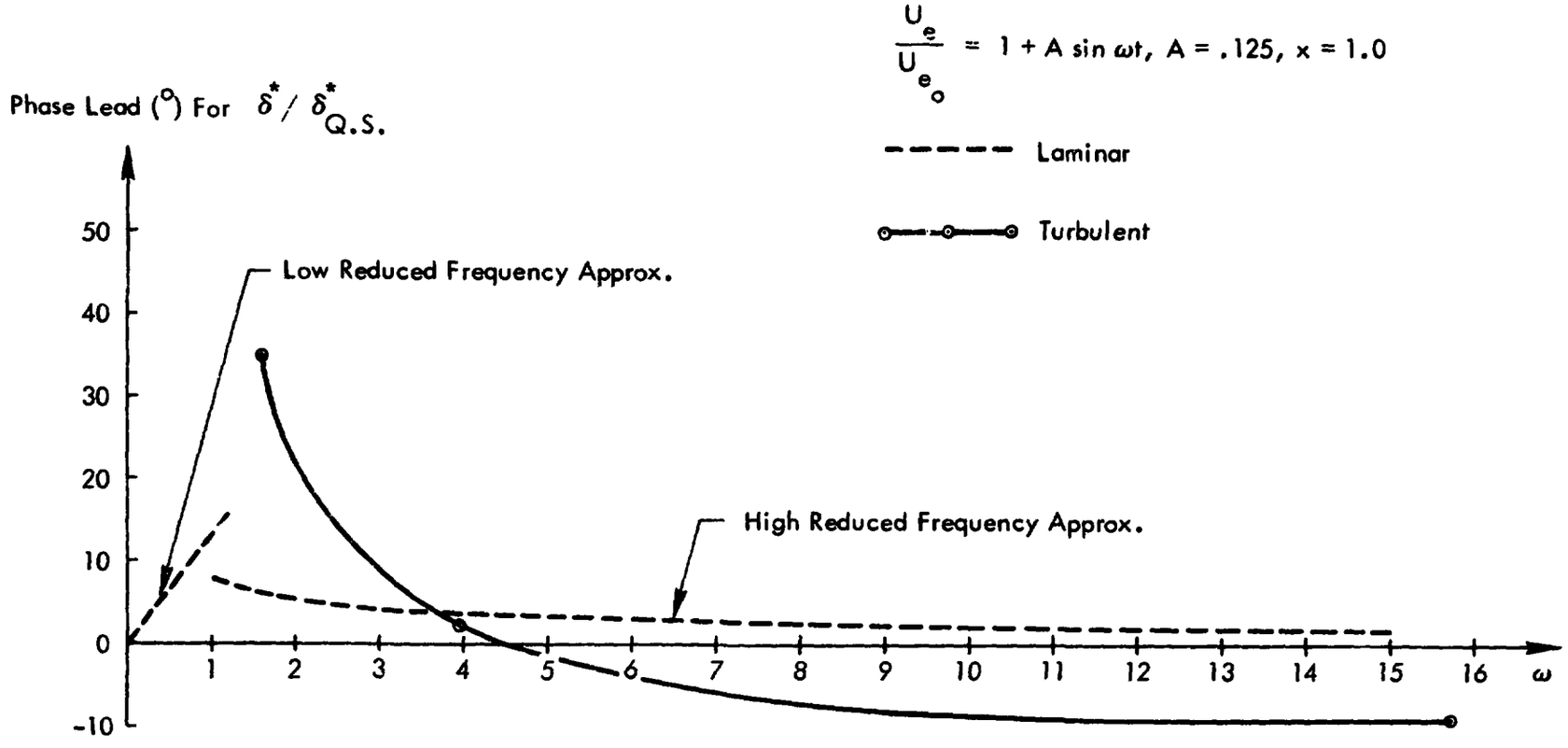

Figure 11. Displacement Thickness Phase Lead Vs. Reduced Frequency for Laminar and Turbulent Flow

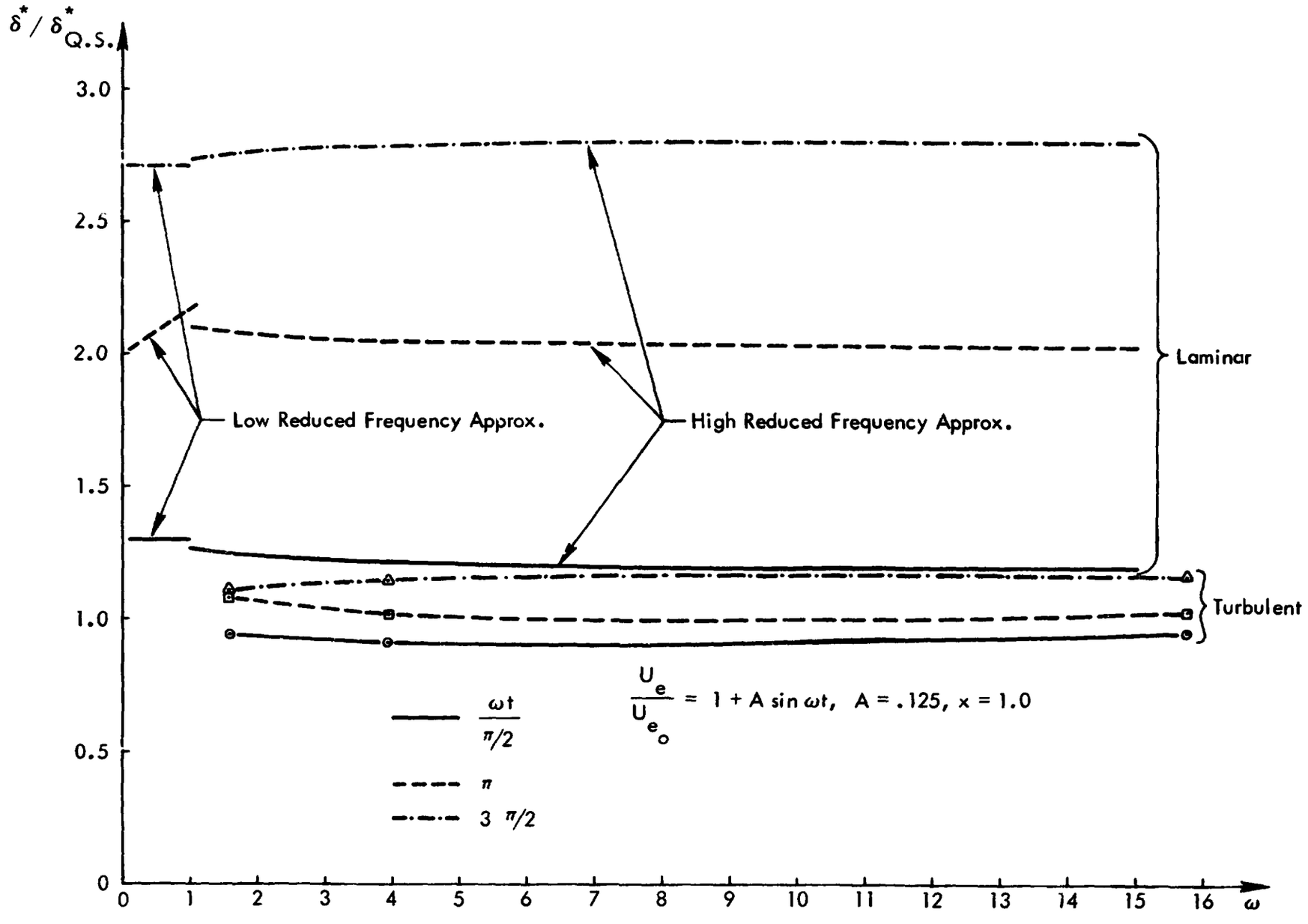

Figure 12. Displacement Thickness Vs. Reduced Frequency for Laminar and Turbulent Flow

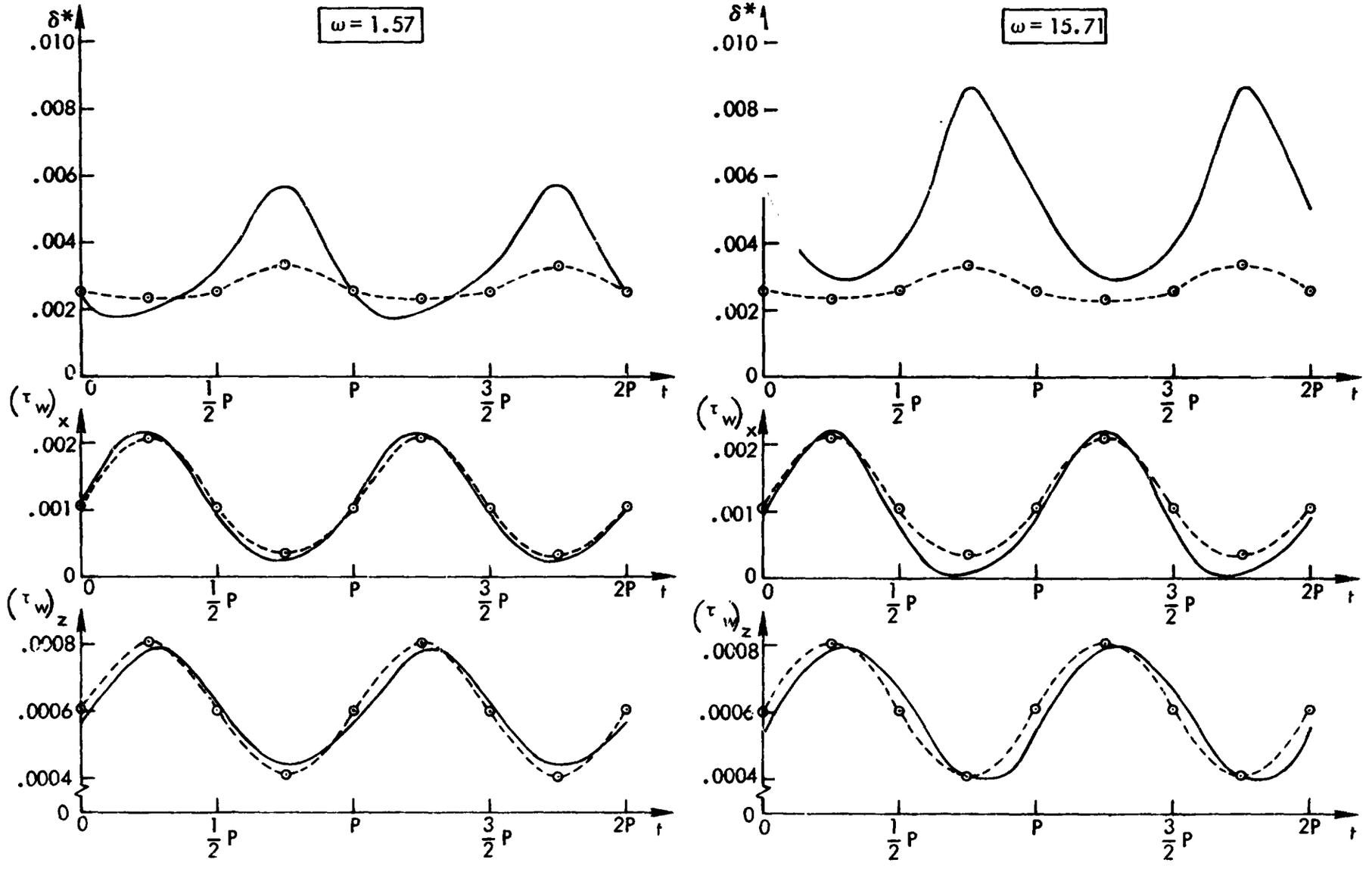

Figure 13. Oscillatory Flow Over 30° Swept Flat Plate At High Amplitude

$$\frac{U_e}{U_{e_o}} = 1 + (A_o + A_1 \sin \omega t)\, x;\quad A_o = -.2 \quad A_1 = .1,\ x = 1.0$$

o-o-o Quasi-Steady

+-+-+ High Frequency Approx.

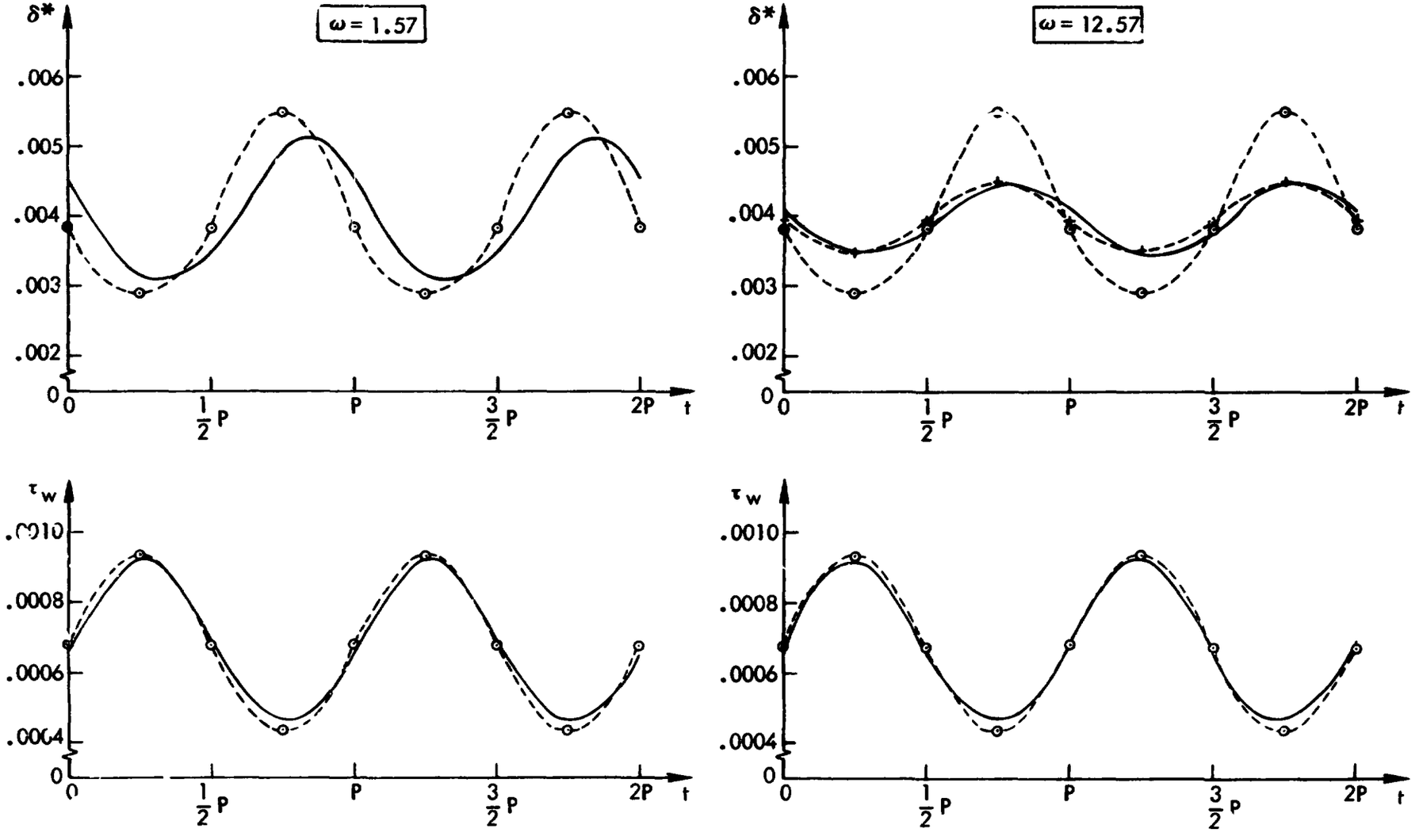

Figure 14. Oscillatory Retarded Flow at Low Amplitude

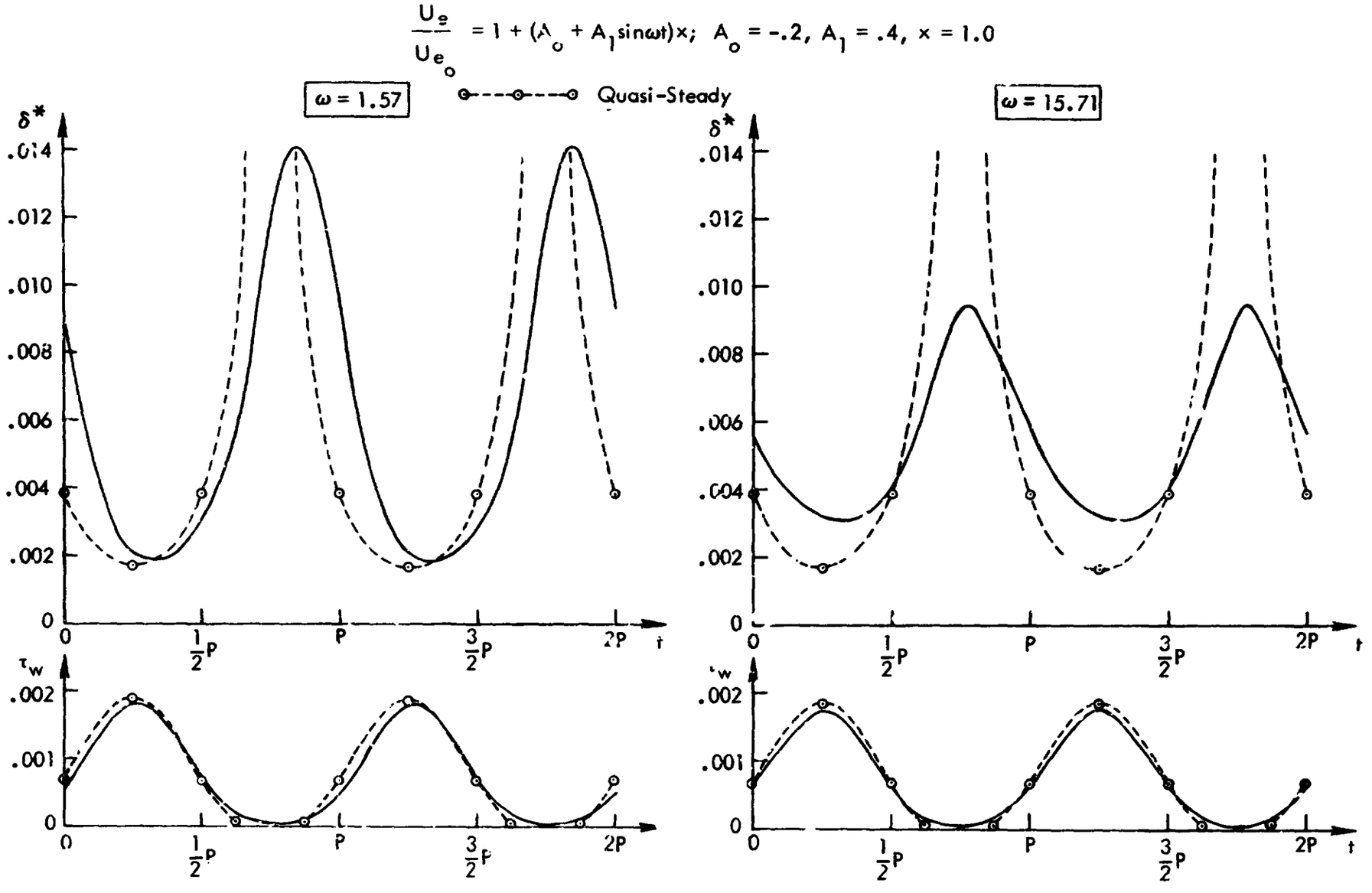

Figure 15. Oscillatory Retarded Flow at High Amplitude

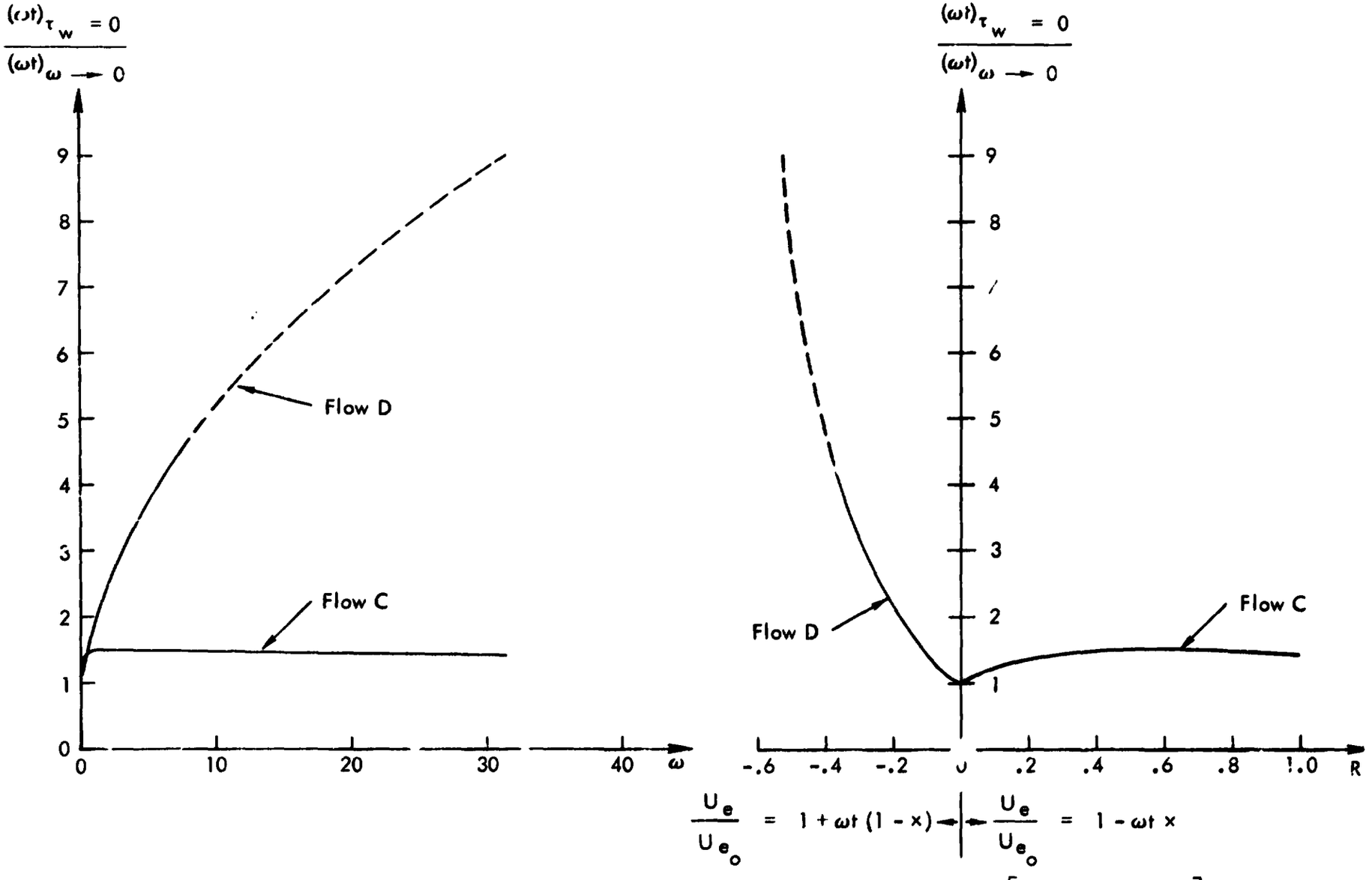

Figure 16. Variation of Velocity Gradient Magnitude for Zero Wall Shear Stress at Trailing Edge with Frequency and with Ratio, R

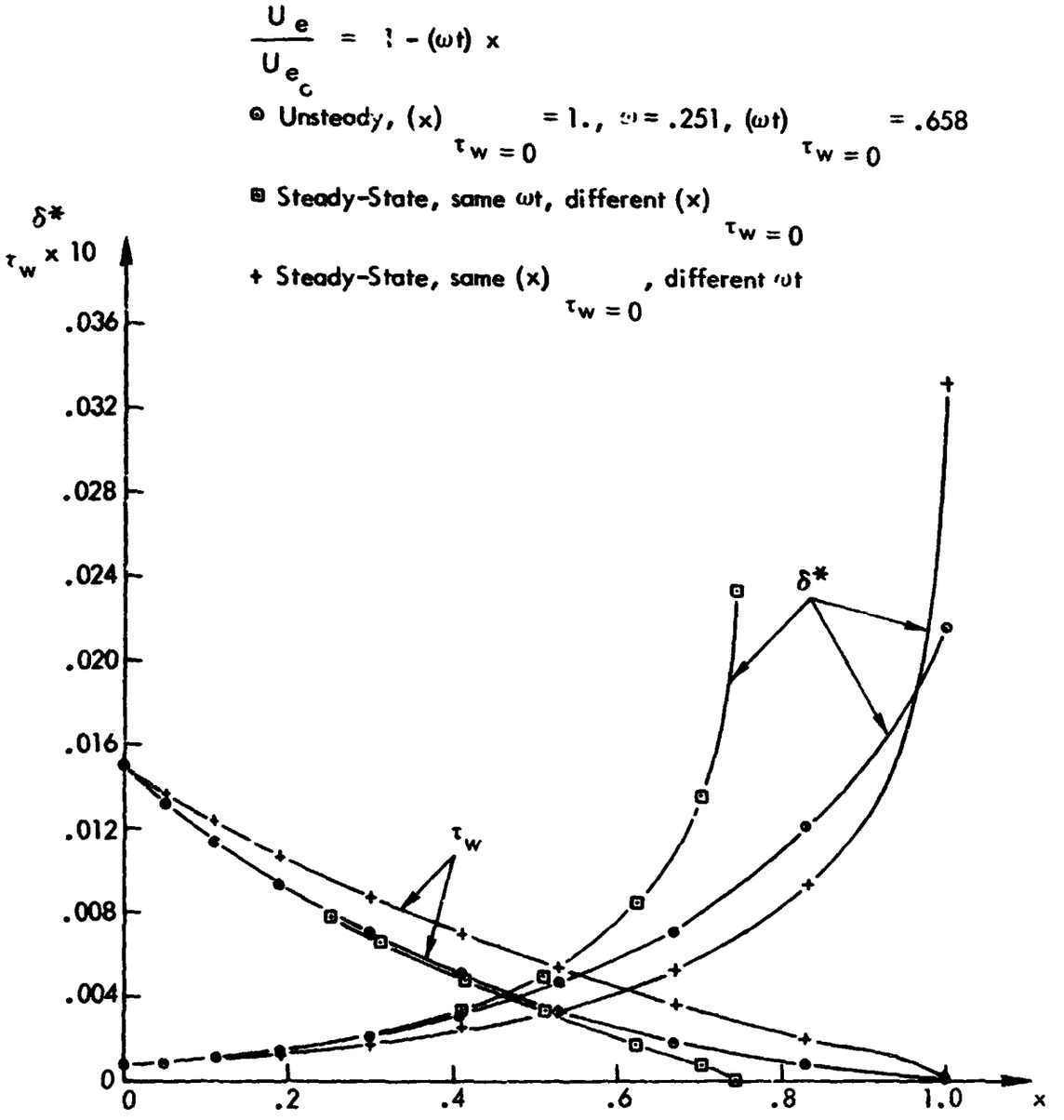

Figure 17. Wall Shear Stress and Displacement Thickness Distribution for Flow C at Low Frequency

$$\frac{U_e}{U_{e_o}} = 1 - (\omega t)\, x$$

⊙ Unsteady, $(x)_{\tau_w = 0} = 1.0$, $\omega = 31.416$, $(\omega t)_{\tau_w = 0} = .682$

⊡ Steady-State, same ωt, different $(x)_{\tau_w = 0}$

x Steady-State, same $(x)_{\tau_w = 0}$, different ωt

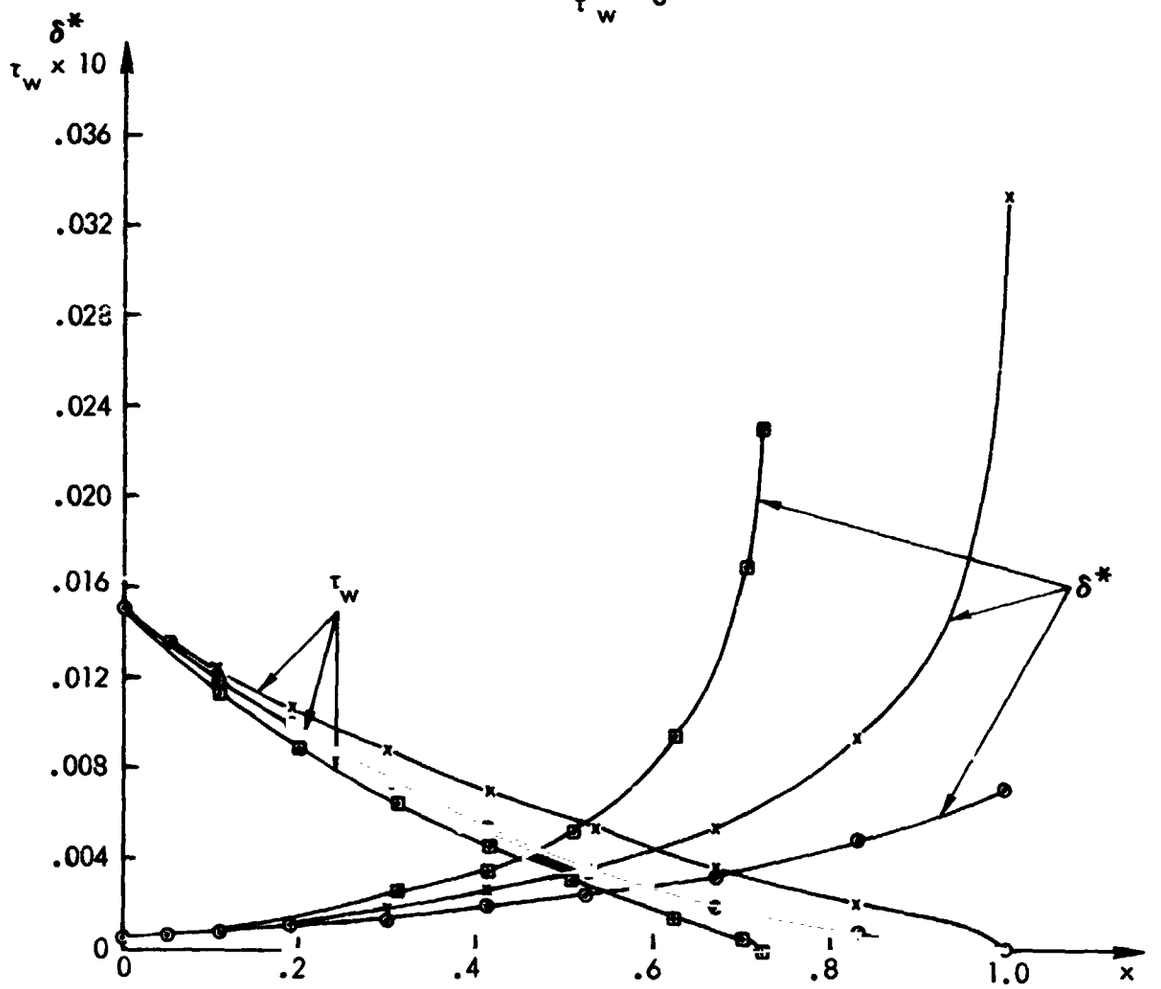

Figure 18. Wall Shear Stress and Displacement Thickness Distribution for Flow C at High Frequency

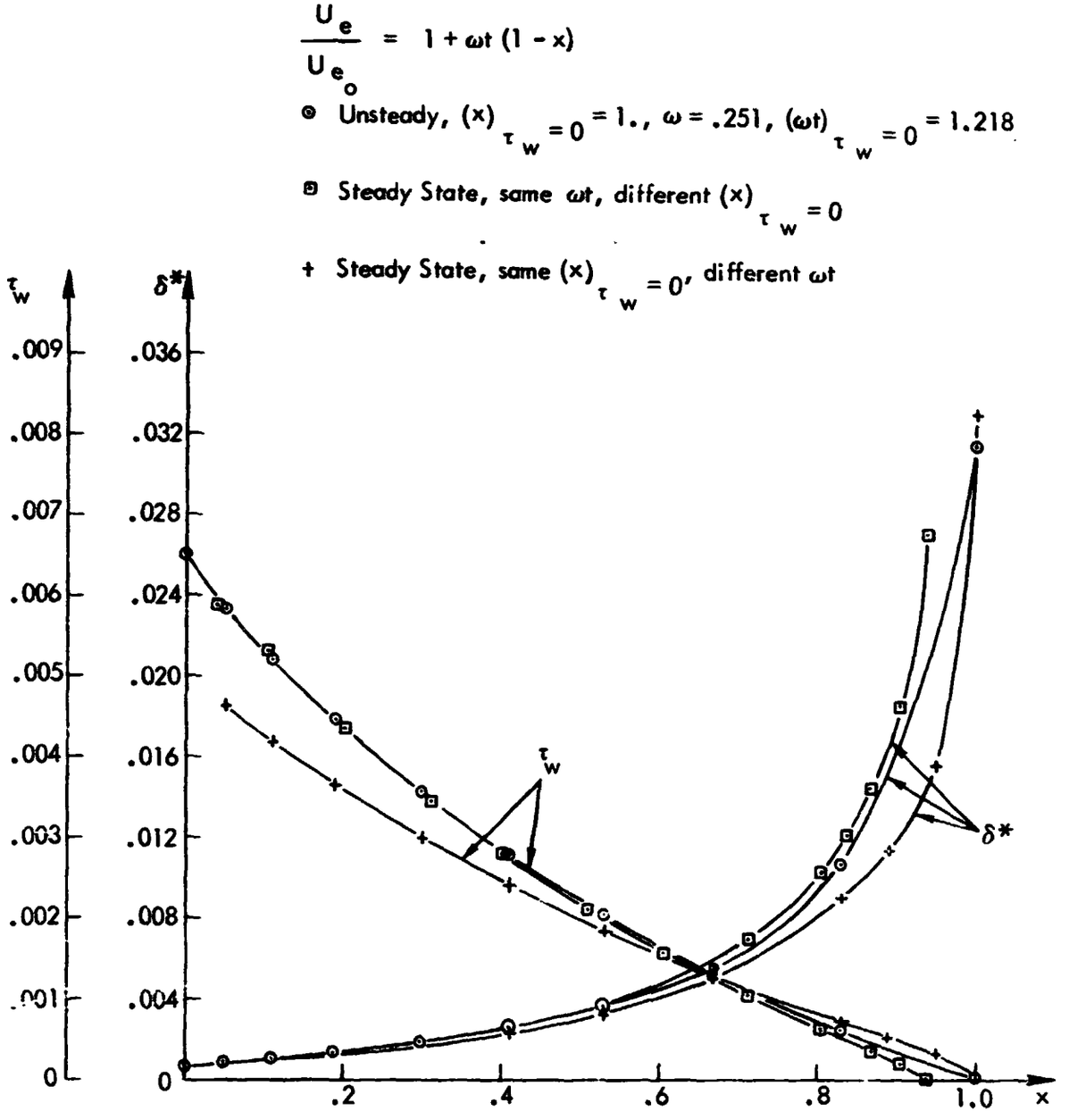

Figure 19. Wall Shear Stress and Displacement Thickness Distribution for Flow D at Low Frequency

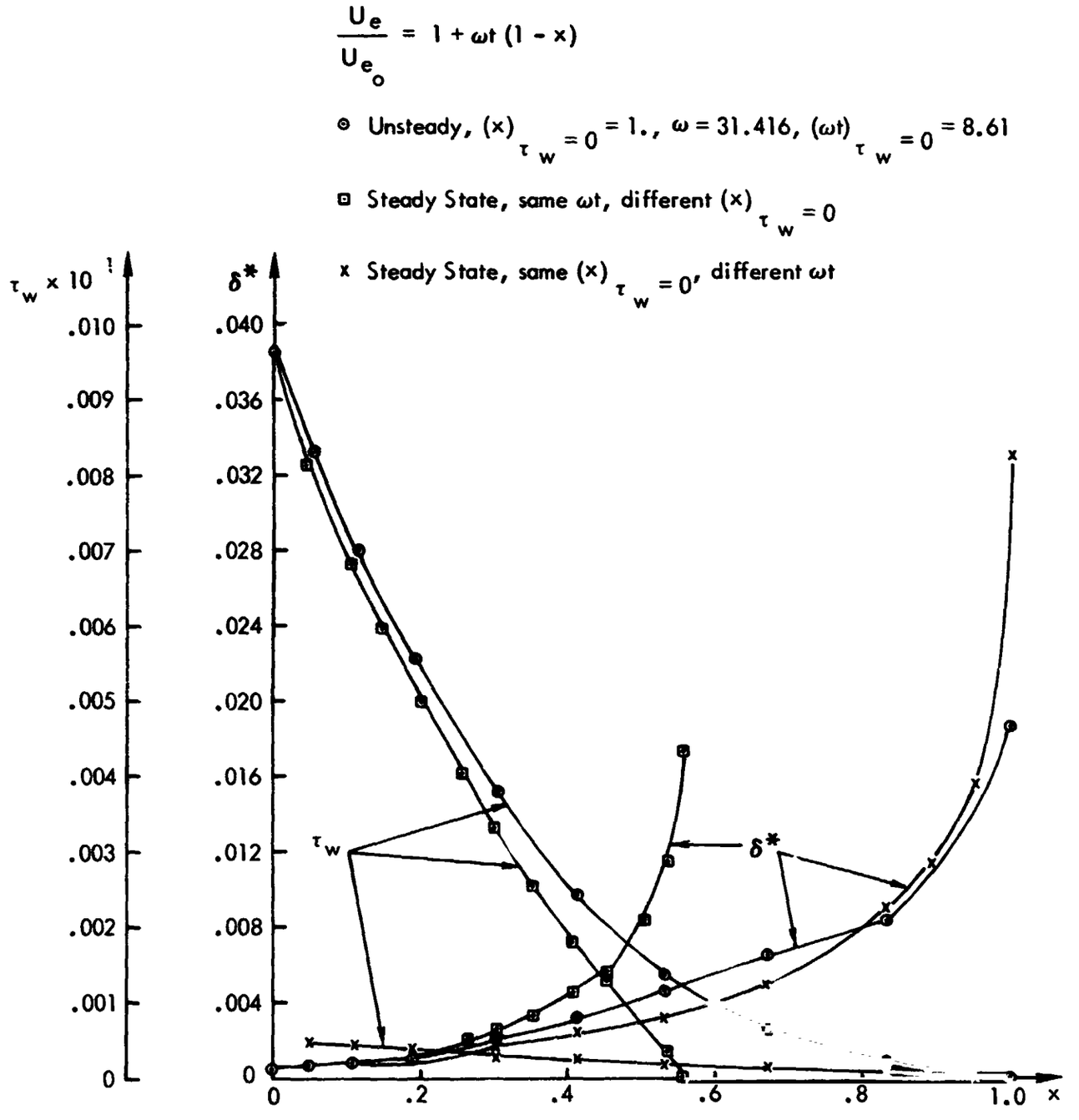

Figure 20. Wall Shear Stress and Displacement Thickness Distribution for Flow D at High Frequency

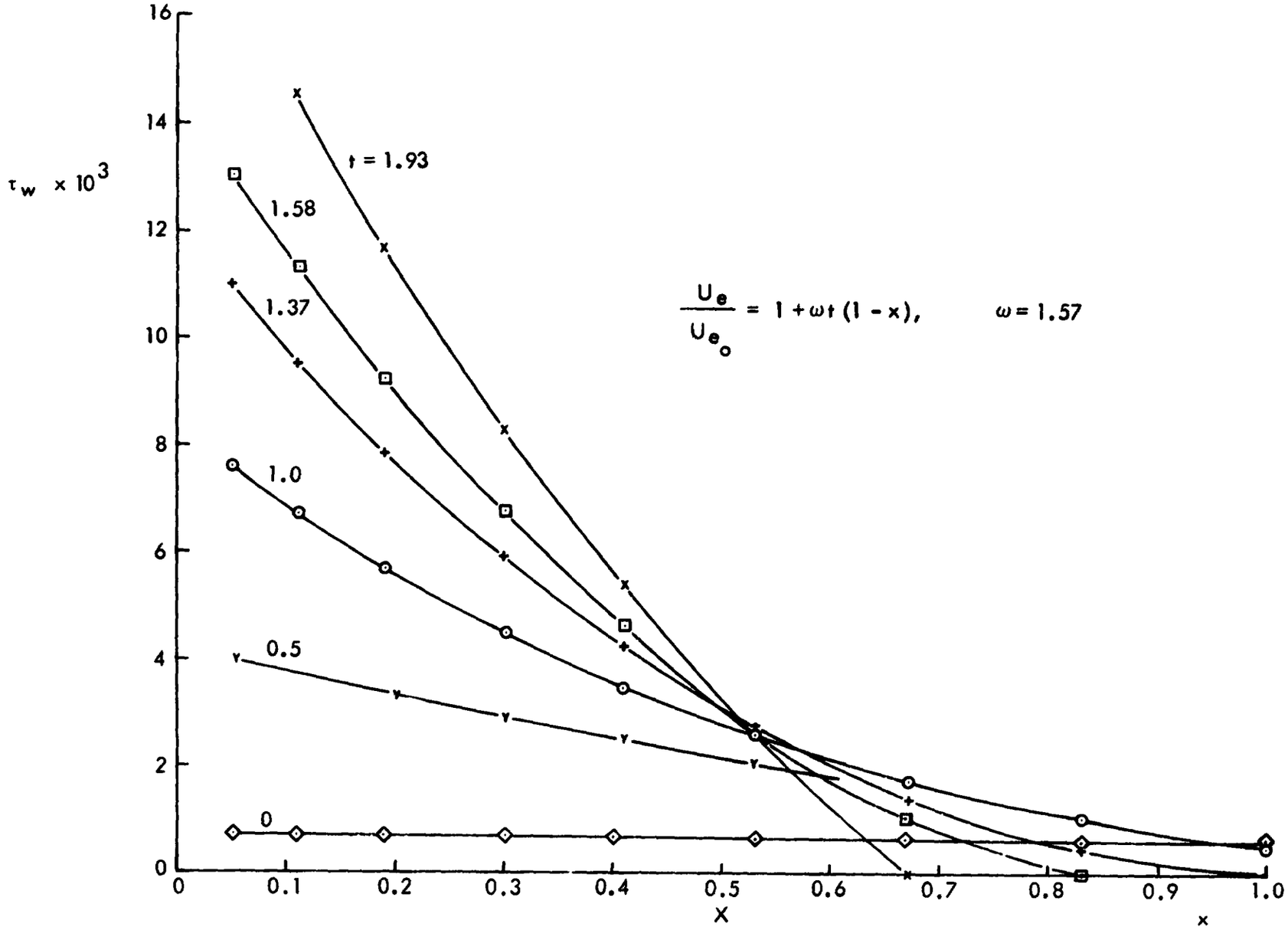

Figure 21. Development of the Wall Shear Stress; Flow D

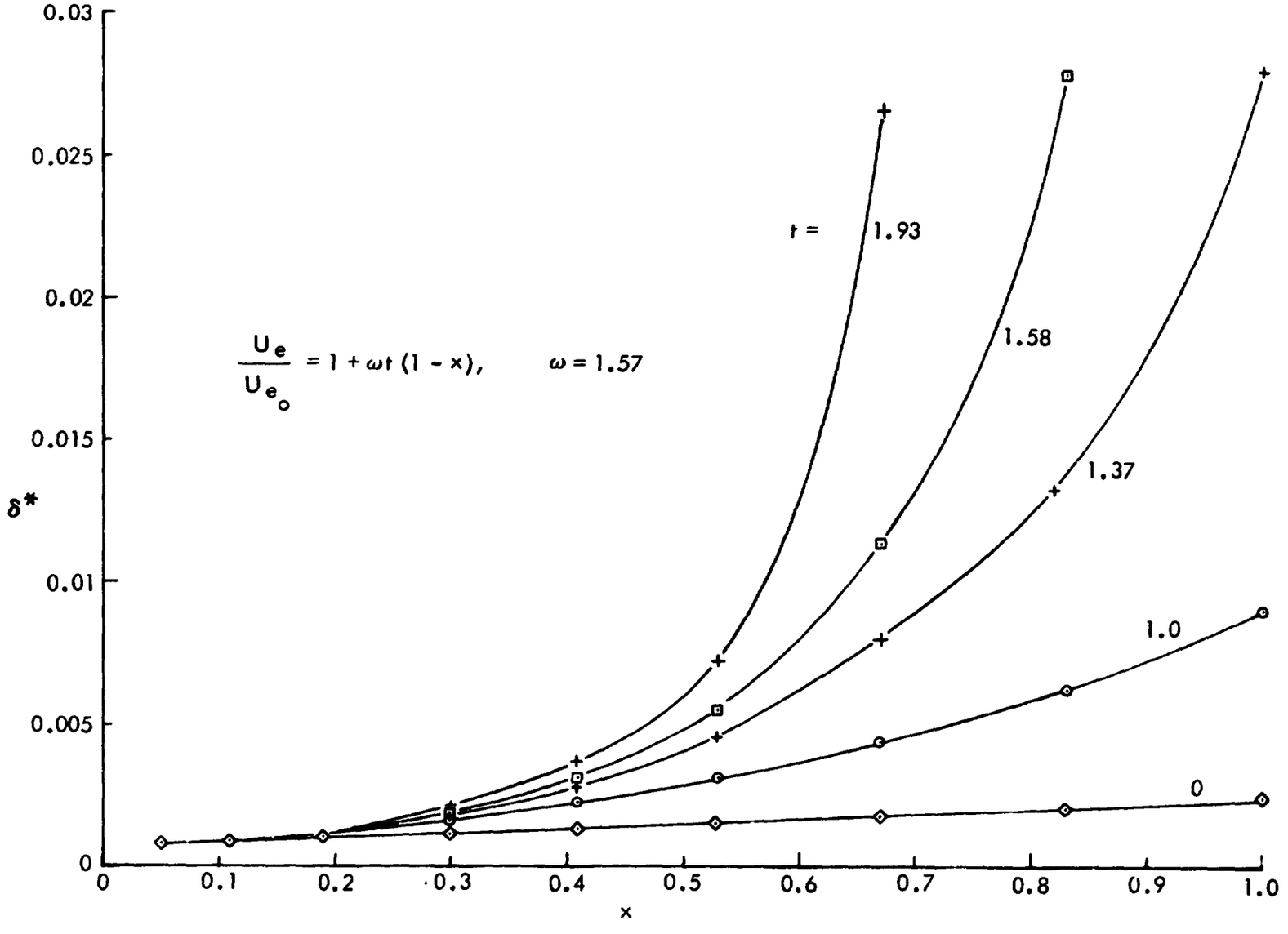

Figure 22. Development of the Displacement Thickness; Flow D

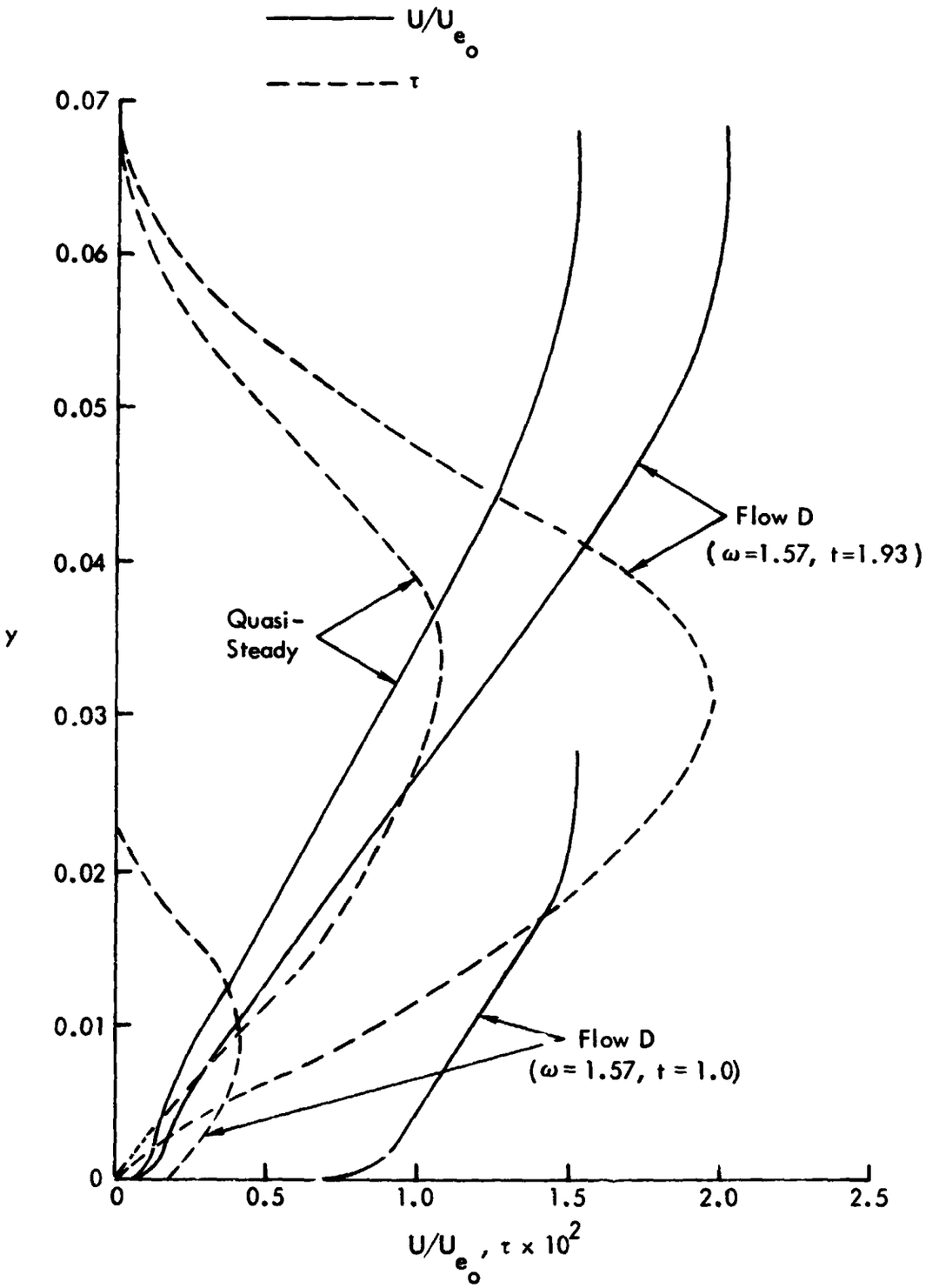

Figure 23. Velocity and Shear-Stress Profiles at x = 0.67; Comparison Between Flow D and Quasi-Steady Flow.

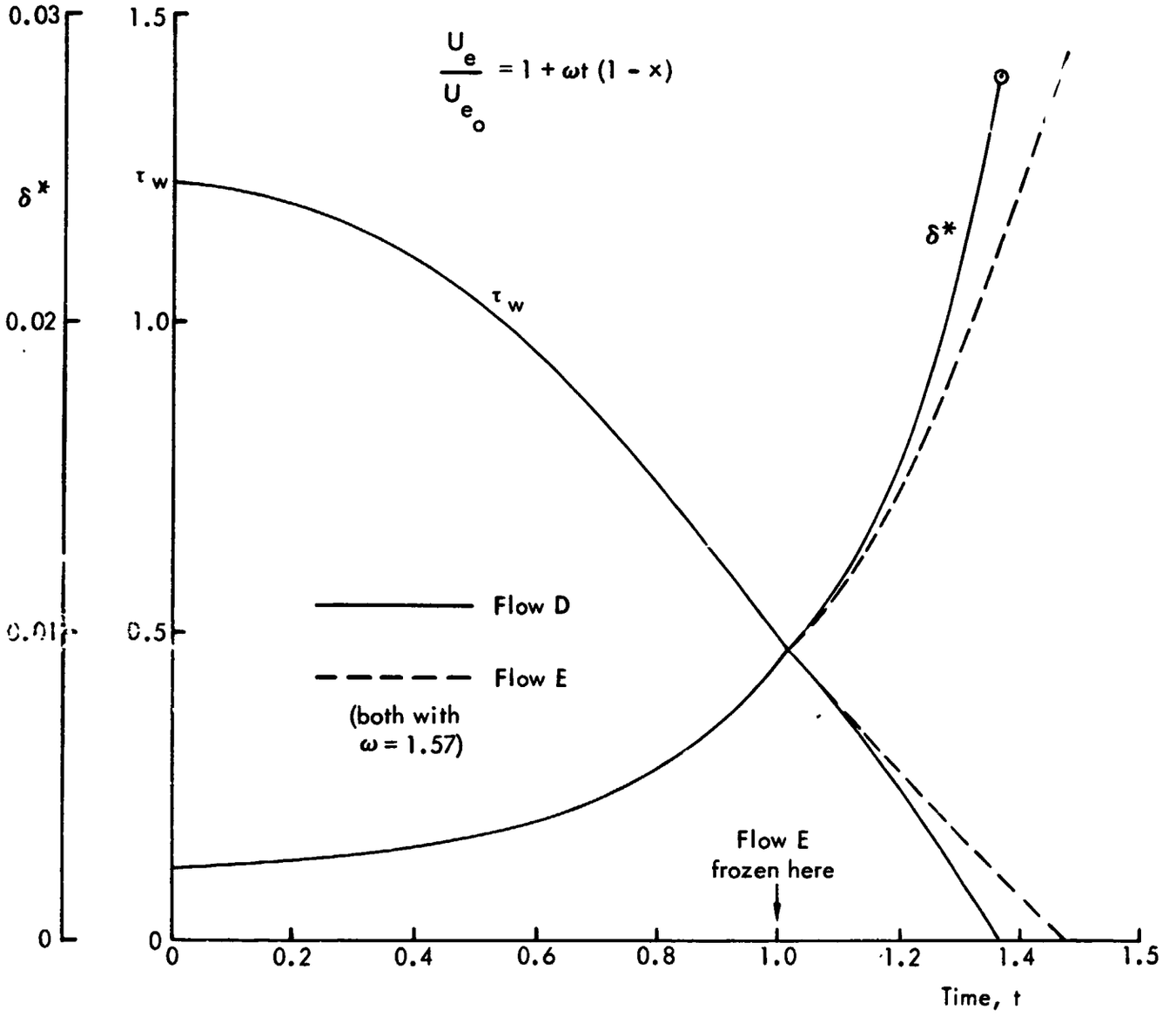

Figure 24. Development of Displacement Thickness and Wall Shear Stress at x = 1

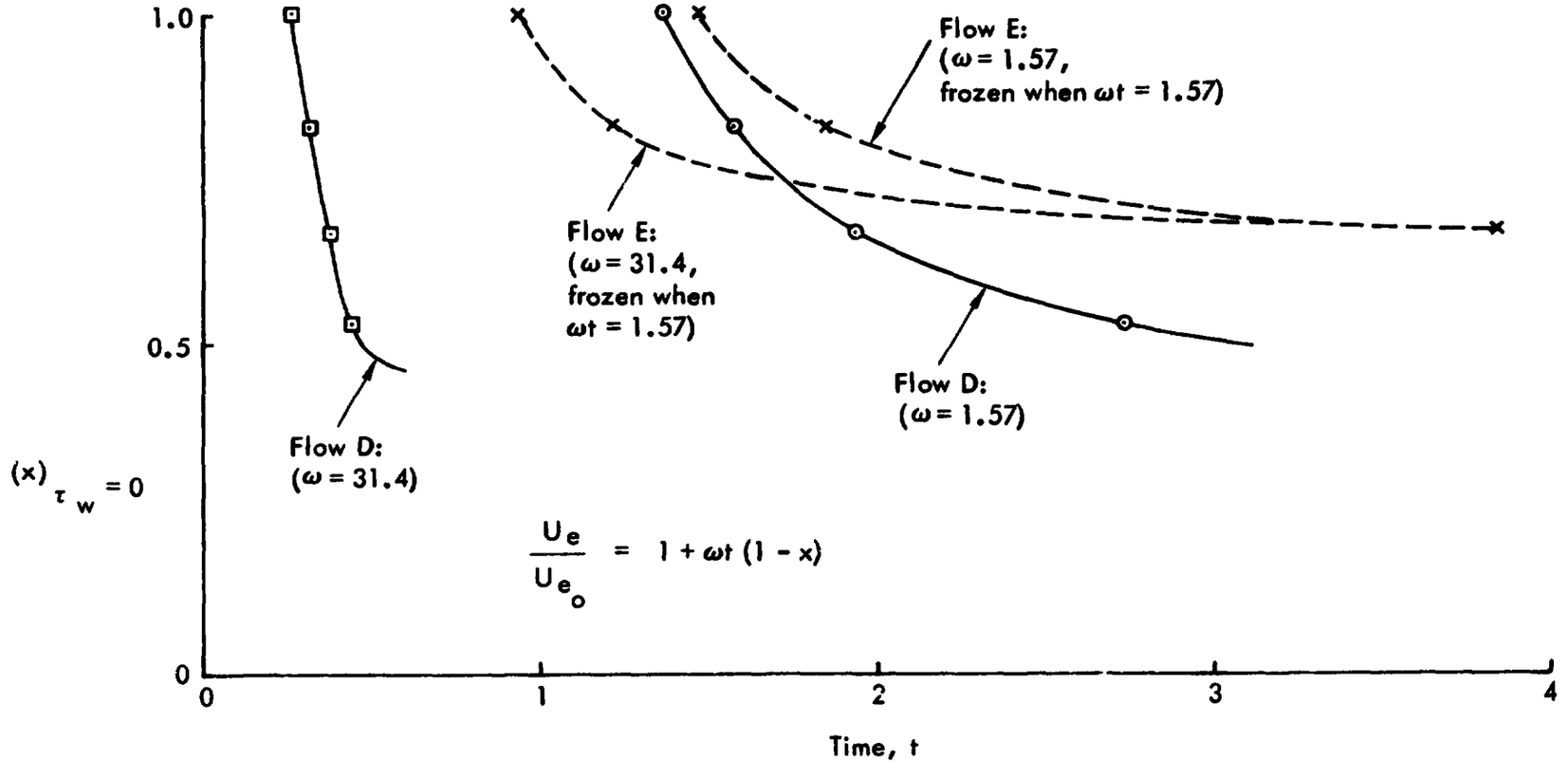

Figure 25. Upstream Movement of the Point of Zero Wall Shear Stress; Flows D and E.

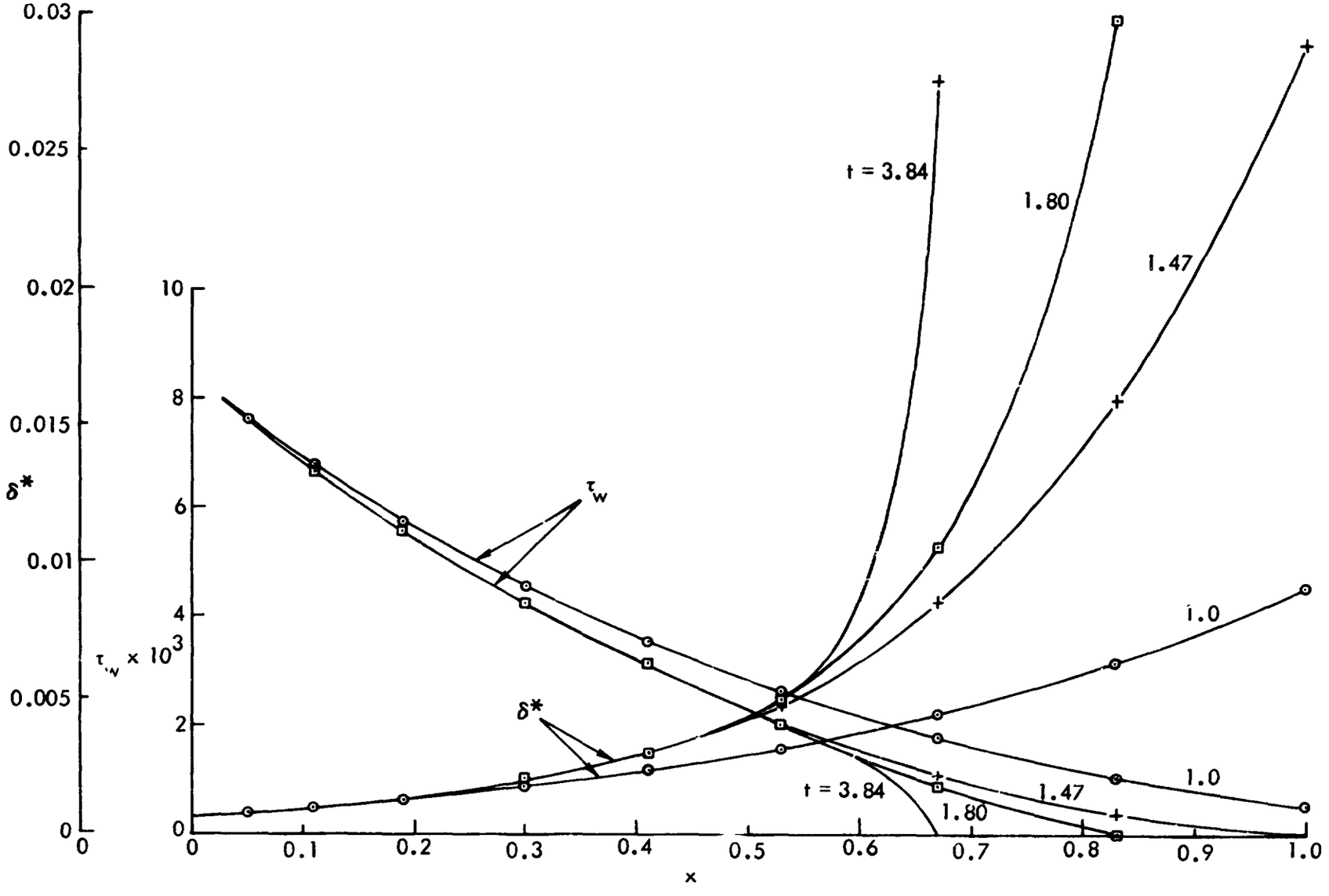

Figure 26. Development of Displacement Thickness and Wall Shear Stress; Flow E ($\omega = 1.57$, frozen when $t = 1.0$)

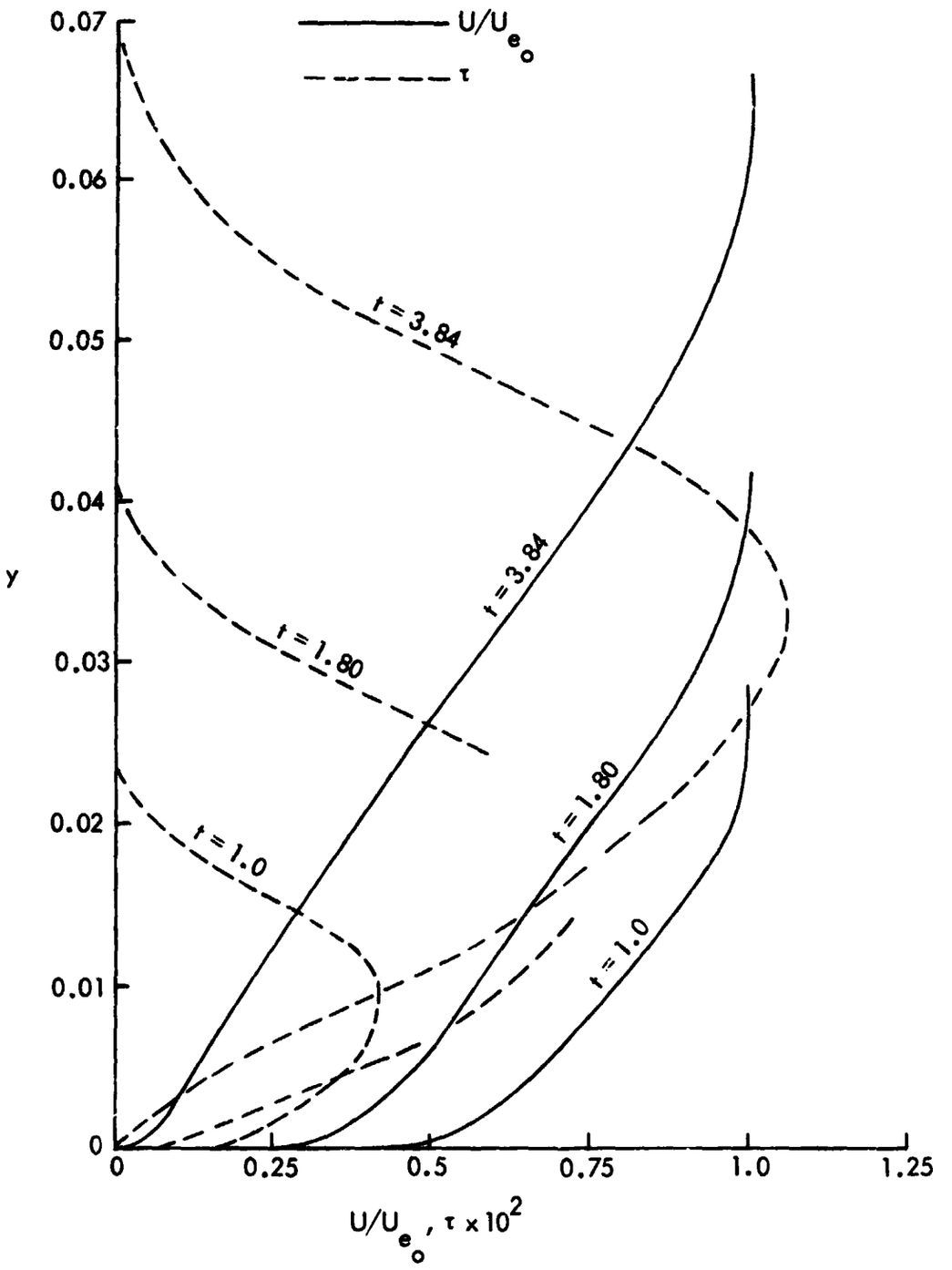

Figure 27. Development of Velocity and Shear-Stress Profiles at x=0.67; Flow E (ω = 1.57, Frozen When t = 1.0)

REFERENCES

1. J. G. Hicks and J. F. Nash, "The Calculation of Three-Dimensional Turbulent Boundary Layers on Helicopter Rotors," NASA CR-1845, May 1971.

2. V. C. Patel and J. F. Nash, "Some Solutions of the Unsteady Turbulent Boundary Layer Equations," IUTAM Symposium on Unsteady Boundary Layers, Quebec, Canada, 1971.

3. H. McDonald and S. J. Shamroth, "An Analysis and Application of the Time-Dependent Turbulent Boundary-Layer Equations," AIAA Journal, Vol. 9, No. 8, August 1971, pp. 1553-1560.

4. P. Bradshaw, "Calculation of Boundary Layer Development Using the Turbulent Energy Equation. VI Unsteady Flow," NPL Aero Report 1288, Feb. 1969.

5. D. E. Abbott and T. Cebeci, "The General Analysis of Unsteady Boundary Layers - Laminar and Turbulent," in Fluid Dynamics of Unsteady, Three-Dimensional and Separated Flows, Proceedings of a Project SQUID Workshop, Georgia Institute of Technology, June 10 - 11, 1971, Ed. by F. J. Marshall.

6. J. F. Nash and V. C. Patel, Three-Dimensional Turbulent Boundary Layers, SBC Technical Books, 1972.

7. J. F. Nash and V. C. Patel, "A Generalized Method for the Calculation of Three-Dimensional Turbulent Boundary Layers," in Fluid Dynamics of Unsteady, Three-Dimensional and Separated Flows, Proceedings of a Project SQUID Workshop, Georgia Institute of Technology, June 10 - 11, 1971, Ed. by F. J. Marshall.

8. J. F. Nash, "An Explicit Scheme for the Calculation of Three-Dimensional Turbulent Boundary Layers," J. Basic Eng. 94D, p. 131, March 1972.

REFERENCES (Cont'd)

9. M. J. Lighthill, "The Response of Laminar Skin Friction and Heat Transfer to Fluctuations in the Stream Velocity," Proc. Roy. Soc. A224, p. 1, 1954.

10. W. R. Sears, "Unsteady Boundary-Layer Separation," IUTAM Symposium on Unsteady Boundary Layers, Quebec, Canada, 1971.